U.S. Department of Energy
Energy Efficiency and Renewable Energy
Bringing you a prosperous future where energy is clean, abundant, reliable, and affordable

Industrial Technologies Program

Industrial Materials for the Future

Final Technical Report

Predicting Pattern Tooling and Casting Dimensions for Investment Casting, Phase III

December 2007

Principal Investigators:

Nick Cannell
Edison Materials Technology Center

Adrian S. Sabau
Oak Ridge National Laboratory

Managed by
UT-Battelle, LLC

ORNL/TM-2007/204

FINAL TECHNICAL REPORT

Project Title: Predicting Pattern Tooling and Casting Dimensions for Investment Casting, Phase III

DOE Award Number: DE-FC36-04GO14230

Project Period: June 1, 2004–September 30, 2007

PI(s):

Nick Cannell (EMTEC)
(216) 408-7706
ncannell@gmail.com

Adrian S. Sabau (ORNL)
(865) 241-5145
sabaua@ornl.gov

Recipient Organization:

Edison Materials Technology Center (EMTEC)
3155 Research Blvd.
Kettering, OH 45420

National Laboratory:

Oak Ridge National Laboratory

Project Team:

Contact	Company
Bill Schrey	Schrey & Sons Mold
Bob Dzugan	Buycastings.com
Bob Horton	Precision Metalsmiths, Inc.
James A. Oti	J & J, a DePuy Company
Jerry Donohue	Precision Colloids, LLC
Jerry Kovatch	Precision Metalsmiths, Inc.
Jerry Snow	Minco, Inc.
Jim Gardner	JEM Mfg.
Nip Singh	S & A Consulting Group, LLP
Timothy Wolff	Argueso & Co.
Mike Payne	Precision Castings, Inc.
Nick Cannell	EMTEC

ORNL/TM-2007/204

Predicting Pattern Tooling and Casting Dimensions for Investment Casting, Phase III

Nick Cannell
Edison Materials Technology Center

Adrian S. Sabau
Oak Ridge National Laboratory

October 2007

Prepared by
OAK RIDGE NATIONAL LABORATORY
P.O. Box 2008
Oak Ridge, Tennessee 37831-6283
managed by
UT-Battelle, LLC
for the
U.S. DEPARTMENT OF ENERGY
under contract DE-AC05-00OR22725

Acknowledgments and Disclaimer

Acknowledgments

This report is based upon work supported by the U.S. Department of Energy, Energy Efficiency and Renewable Energy, Industries of the Future - Metal casting, under Award No. DE-FC36-04GO14230.

We would like to thank Srinath Viswanathan of ORNL, who initiated phase I of the project, M. Argueso & Co., Inc., for providing the wax for this study; T. Wolf, P. A. Silverstein, W. R. Fricker, and I. Al-Rabadi of Argueso for assistance with the wax injection experiments; M. Radovic and R.M. Trejo of ORNL, for conducting rheometry measurements on filled waxes at HTML/ORNL, and W.D. Porter of ORNL for conducting high temperature dilatometry measurements for 17-4PH alloy.

Thanks also go to J. Snow, D. Scott, and B. Sneider of Minco, Inc., for shell investment and for embedding thermocouples within the shell; E. Hatfield for casting assistance; Z. Wu, a University of Tennessee graduate student, for obtaining the shrinkage factors from measured dimensions; J. Kovatch and R. Abramczyk of Precision Metalsmiths, Inc. (PMI), for conducting casting experiments; Allen Bransford and Mike Payne, Precision Castings of Tennessee, Inc., for providing access to their foundry; B. Schrey, of Schrey & Sons Mold Co., for providing the sprue tooling; and Jim Gardner, J.E.M. Manufacturing, for casting design, providing wax patterns for the sprue, designing and coordinating the fabrication of a test bar, and coordinating wax injection, shell making, and casting at PCC, Inc., Viking Metalgraphics, Inc., and SeaCast, Inc; Schrey & Sons, Inc and McCaughin, Inc. for providing the test bar wax patterns, Remet, Inc. for providing waxes, and Dr. G. M. Rowe of Abatech, Inc. for conducting DMA experiments and determining the discrete relaxation spectra for the torsion DMA data set, H. Lobo and T. Bethard of Datapoint Labs, Inc., for conducting DSC and thermal conductivity measurements.

Disclaimer

Contents

List of Figures

List of Tables

Abbreviations, Acronyms, and Symbols

ABAQUS	computer simulation program
17-4PH	steel
AFS	American Foundry Society
a_s	alloy shrinkage
c_s	casting shrinkage
C1, C2	thermocouples embedded in the shell cavity
CMM	coordinate measurement machine
DSC	differential scanning calorimeter
DTA	differential thermal analysis
EMTEC	Edison Materials Technology Center
HTC	heat transfer coefficient, W/m^2K
ICI	Investment Casting Institute
k	thermal conductivity
L2-5, L25	length between steps 2 and 5
ORNL	Oak Ridge National Laboratory
PCT	Precision Casting of Tennessee, Inc.
ProCAST	casting simulation software
PMI	Precision Metalsmiths, Inc.
T	temperature, units indicated in graphs or tables
w_s	wax shrinkage

1. Executive Summary

The investment casting process allows the production of complex-shape parts and close dimensional tolerances. One of the most important phases in the investment casting process is the design of the pattern die. Pattern dies are used to create wax patterns by injecting wax into dies. The wax patterns are used to create a ceramic shell by the application of a series of ceramic coatings, and the alloy is cast into the dewaxed shell mold (Fig. 1.1). However, the complexity of shape and the close dimensional tolerances required in the final casting make it difficult to determine tooling dimensions.

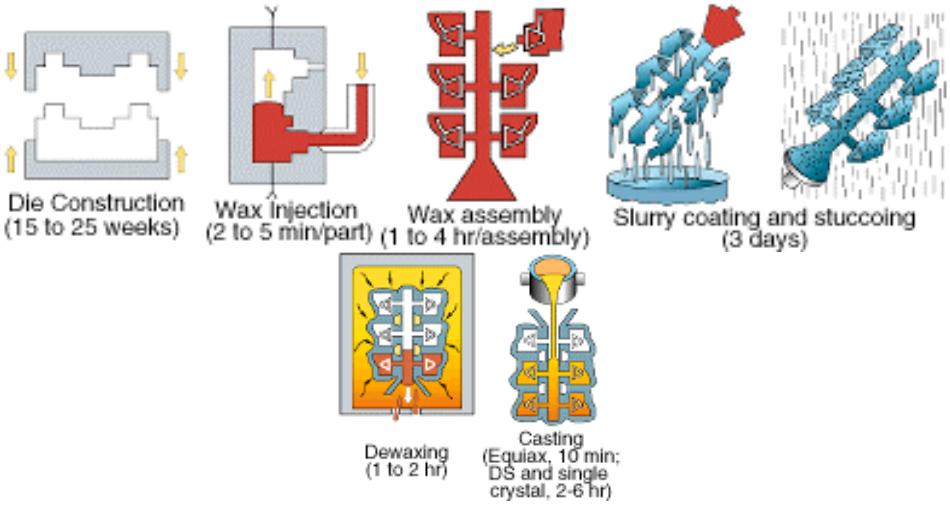

Fig. 1.1. Sketches of the investment casting process (schematic from http://www.machinedesign.com).

In most cases, the mold geometry or cores restrict the shrinkage of the pattern or the cast part, and the final casting dimensions may be affected by time-dependent processes such as viscoelastic deformation of the wax, and viscoplastic creep and plastic deformations of the shell and alloy (Fig. 1.2). The pattern die is often reworked several times to produce castings whose dimensions are within acceptable tolerances.

1.1 Project Goal

The goal of this project was to predict casting dimensions for investment castings in order to meet blueprint nominal during the first casting run. Several interactions have to be considered in a coupled manner to determine the shrinkage factors: these are the die-wax, wax-shell, and shell-alloy interactions (as illustrated in Fig. 1.3). In this work, the deformations of the die-wax and shell-alloy systems were considered in a coupled manner. Future work is needed in order to deliver to industry a computer program in which all three systems are coupled for determining the dimensions of the wax pattern, the shell mold, and casting in a sequential but coupled manner.

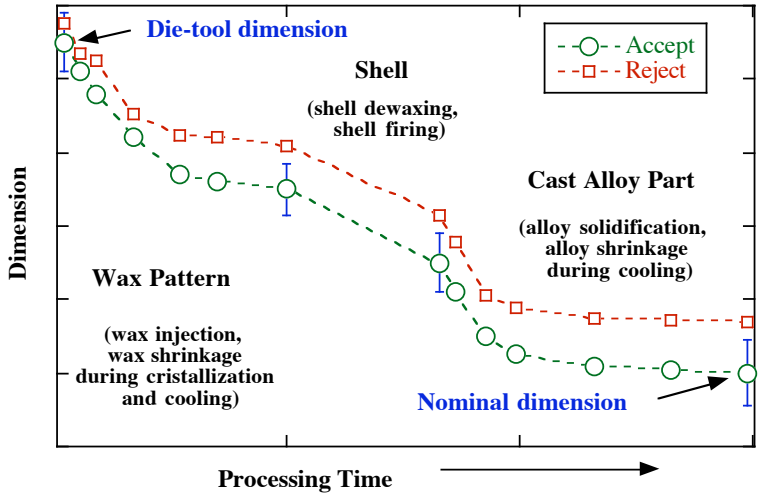

Fig. 1.2. Dimensions in the investment casting process.

Thermo-*physical* properties (tests, data, model) —> Temperature —> ***Thermal expansion***

Thermo-*mechanical* properties (tests, data, model) —> ***Stress and displacement***

Thermal expansion
Stress and displacement
} —> ***Dimensions***

Fig. 1.3. Flow chart illustrating the steps necessary for obtaining the dimensions and ensuing shrinkage factors based on computer models.

1.2 Summary of Project Achievements

Phase I

The first part of the project involved preparation of reports on the state of the art for die-wax, wax-shell, and shell-alloy processes. The primary R&D focus during Phase I was on the wax material since the least was known about it. The main R&D accomplishments during this phase were determination of procedures for obtaining the thermal conductivity and viscoelastic properties of an unfilled wax and validating those procedures.

Phase II

Efforts during Phase II focused on die-wax and shell-alloy systems. A wax material model was developed, and a die-wax model was successfully incorporated into and used in commercial computer programs. At that time, computer simulation programs had complementary features. A viscoelastic module was available in ABAQUS but unavailable in ProCAST, while the mold-filling module was available in ProCAST but unavailable in ABAQUS. Thus, the numerical simulation results were only in good qualitative agreement with experimental results, the predicted shrinkage factors being approximately 2.5 times larger than those measured. Significant progress was made, and results showed that the testing and modeling of wax material had great potential for industrial applications.

Additional R&D focus was placed on the fused-silica shell mold and A356 aluminum alloy system. The experimental part of the program was conducted at ORNL and commercial foundries, where wax patterns were injected, molds were invested, and alloys were poured. Significant effort was made to obtain temperature profiles in the shell mold. A model for thermal radiation within the shell mold was developed, and the thermal model was successfully validated using ProCAST. The alloy dimensions were obtained from numerical simulations only with coupled shell-alloy systems. The A356 alloy dimensions were in excellent quantitative agreement with experimental data, validating the deformation module.

Phase III: Current Project

Efforts during Phase III focused mainly on the shell-alloy systems. A high melting point alloy, 17-4PH stainless steel, was considered. The experimental part of the program was conducted at ORNL and commercial foundries, where wax patterns were injected, molds were invested, and alloys were poured. Shell molds made of fused silica and alumino-silicates were considered. A literature review was conducted on thermophysical and thermomechanical properties alumino-silicates. Material property data, which were not available from material suppliers, was obtained.

For all the properties of 17-4PH stainless steel, the experimental data available in the literature did not cover the entire temperature range necessary for process simulation. Thus, some material properties were evaluated using ProCAST, based on CompuTherm database. A comparison between the predicted material property data and measured property data was made. It was found that most material properties were accurately predicted only over several temperature ranges. No experimental data for plastic modulus were found. Thus, several assumptions were made and ProCAST recommendations were followed in order to obtain a complete set of mechanical property data at high temperatures. Thermal expansion measurements for the 17-4PH alloy were conducted during heating and cooling. As a function of temperature, the thermal expansion for both the alloy and shell mold materials showed different evolution on heating and cooling.

Numerical simulations were performed using ProCAST for the investment casting of 17-4PH stainless steel parts in fused silica molds using the thermal expansion obtained on heating and another one with thermal expansion obtained on cooling. Since the fused silica shells had the lowest thermal expansion properties in the industry, the dewaxing phase, including the coupling between wax-shell systems, was neglected. The shell mold was considered to be a pure elastic material. The alloy dimensions were obtained from numerical simulations. For 17-4PH stainless steel parts, the alloy shrinkage factors were over-predicted, as compared with experimental data.

Additional R&D focus was placed on obtaining material property data for filled waxes, waxes that are common in the industry. For the first time in the investment casting industry, the thermo-mechanical properties of unfilled and filled waxes were measured. Test specimens of three waxes were injected at commercial foundries. Rheometry measurement of filled waxes was conducted at ORNL. The analysis of the rheometry data to obtain viscoelastic properties was not completed due to the reduction in the budget of the project (approximately 50% and 60% of DOE funds and cost-share from industrial partners were received, respectively).

1.3 Technology Transfer

The techniques developed in the program were documented in several publications and conference presentations. Detailed reports on alloy and shell mold materials were also issued to the participating companies. Through the ORNL work conducted in this project, the areas of material property

measurement and modeling of material behavior has matured, allowing the software vendors to develop appropriate modules in their codes, the next steps in technology transfer. Over the course of the project, ORNL assisted ProCAST with advice, information, material property data, mesh files, ProCAST setup files.

Recommendations were made to Investment Casting Institute on measurement techniques for waxes. Recommendations for mechanical testing of waxes were made based on testing one unfilled wax and one filled wax, both used by the industry. The recommendations made could be used to establish new testing guidelines for waxes in the investment casting industry.

Commercial adoption of the technologies developed in this program took place through the active participation of the American Foundry Society, Edison Materials Technology Center, and the industrial partners participating in this work. Most of the property data and constitutive equations developed in this program were implemented in ProCAST, the leading casting simulation software for the investment casting industry, allowing immediate dissemination of the information to industry. As a result of this work, ProCAST implemented a viscoelastic module that is currently being tested.

1.4 Recommendations

This project laid the theoretical groundwork for predicting shrinkage factors. Further work on obtaining the alloy mechanical properties at high temperature needs to be performed. Numerical simulations need to be conducted based on more accurate mechanical properties and the accuracy of the deformation module needs to be assessed. Also, the creep properties of the shell molds must also be obtained, modeled, and validated. The analysis of the rheometry data for the filled wax must be completed. The potential for industrial applications of the wax testing must be assessed.

Future work is needed for delivering to the industry a computer program in which the die-wax, wax-shell, and shell-alloy systems are coupled for determining the dimensions of the wax pattern, shell mold, and casting in a sequential but coupled manner.

For technology dissemination, it is now recommended that a new project be started and conducted to incorporate the proposed methodologies into commercial casting software. The software vendors should collaborate with a team of users.

2. Introduction

For the investment casting process, the tooling depends on dimensional changes associated with the wax pattern, ceramic molds, and cast alloys. The nominal casting dimensions can be achieved provided that the die tools were dimensioned with appropriate degree of accuracy. In most cases, the mold geometry or cores restrict the shrinkage of the pattern or the cast part, and the final casting dimensions may be affected by time-dependent processes such as viscoelastic deformation of the wax, and viscoplastic creep and plastic yield of the shell and alloy. Although there is significant information in the literature on these processes, and mathematical models have been developed for continuous and direct chill casting, there has been little or no application to shaped castings. In particular, although many commercial casting codes have stress modules to predict elastic stress, they cannot predict dimensional change or model the effects of geometrical restraint, viscoelastic creep, viscoplastic creep, and plastic yield. These processes occur primarily in investment casting, due to the extended time the casting is at high temperature, and occur to a much lesser extent in other casting processes.

As a step towards predicting tooling dimensions, Sabau (2006) showed that, for the investment casting of aluminum alloys, alloy shrinkage factors were predicted with high degree of accuracy when the deformation of the mold is considered. Wax patterns are made by injecting wax into metal dies, ceramic shells are made by the successive application of ceramic coatings over the wax patterns, and the alloys are cast into the dewaxed shell molds. The dimensional changes associated with wax, shell mold, or alloy, are referred to as wax, shell mold, or alloy shrinkage factors (or tooling allowances), respectively. The usual practice to estimate the die tools' dimensions is by adjusting the nominal casting dimensions with the shrinkage factors.

To date, investment casting technology has been based on hands-on training and experience. Technical literature is limited to experimental, phenomenological studies aimed at obtaining empirical correlations for quick and easy application in industry. The pattern die is often reworked several times to produce castings whose dimensions are within acceptable tolerances. The complexity of shape and the close dimensional tolerances required in the final casting make it difficult to determine the appropriate pattern dimensions with existent casting simulation software except by trial and error.

Improvements in industrial dimensional practices are hindered by (a) the complexity of physical phenomena that determine casting dimensions; (b) the lack of thermophysical property data for the wax, shell, and alloy; and (c) the lack of well-established, validated thermomechanical models that describe the deformation of the wax, shell, and alloy. Although not all of the commercial packages have all the features pertinent to investment casting (e.g., input for radiation heat transfer), most can be used to design gating systems and minimize areas of solidification shrinkage. However, none of the commercial packages can be used for determining the pattern tooling dimensions.

3. Background

The difference between the die dimensions and corresponding casting dimensions are usually referred to as the tooling allowances, or shrinkage factors. To determine the shrinkage factors, the die-wax, wax-shell, and shell-alloy interactions must be considered in a coupled manner.

3.1 Project Approach

The main approach of this project was to determine die tooling dimensions on the basis of material properties and process parameters. Shrinkage factors for the wax pattern, shell mold, and alloy casting were computed; and computational procedures and experimental methodologies were developed.

The technical execution of the project was carried out primarily by research staff at Oak Ridge National Laboratory (ORNL). The Edison Materials Technology Center (EMTEC) and industry participants was closely involved in the dissemination of the technology to the rest of the investment casting and foundry industry through the activities of the American Foundry Society (AFS) 4L Investment Casting Committee, the AFS Congress and ICI.

This program was conducted with substantial involvement by industrial members of the 4L Investment Casting Committee. Industry members determined project deliverables; provided detailed information on wax, shell, and alloy materials and process variables; provided materials for testing; characterized materials; gave technical assistance; conducted experiments needed for model validation; conducted in-plant trials for the validation of developed technologies; and monitored progress.

3.2 Review of Computer Models for Wax, Shell, and Alloy Deformation

Wax deformation (die-wax interaction). At the start of phase III of this project, computer simulation programs for wax deformation had complementary features. A viscoelastic module was available in ABAQUS but unavailable in ProCAST, while the mold-filling module was available in ProCAST but unavailable in ABAQUS. Based on the work performed in phase I and II of this project, ProCAST has implemented a viscoelastic module, which now is being tested.

Shell deformation (wax-shell and shell-alloy interactions). Thermal expansion and shrinkage are the most important properties of the shell. The thermal expansion behavior of shell systems is very well reported in the literature (Straton et al.; Weddington et al., 1990; Snow 1995). Dimensional changes of the shell mold reported in the literature primarily take into account the thermal expansion characteristics of the shell. Computer models are unavailable for the numerical simulation of wax-shell interaction. Computer simulations are available for the shell-alloy systems.

Modeling of alloy deformation (shell-alloy interaction). Data on mechanical properties, which are needed for the numerical simulation of alloy deformation, were not readily available, especially at high temperatures. The experimental data available for the Young's modulus was limited to 900 ^{o}C. As with the thermophysical property data, the thermomechanical property data were measured and reported in several references at relatively low temperatures, i.e., $T < 0.5\ T_S$, where T_S=1,430 ^{o}C is the solidus temperature. The data for yield strength near the solidus were not available and ProCAST recommendations were followed for setting the yield strength at those high temperatures. Plastic models with isotropic hardening are used in continuous casting modeling due to their easy

computational implementation. A more complex treatment for thermo-mechanical behavior is the viscoplastic model, in which the strain rate dependence is considered. Fachinotti and Cardona (2003) reviewed data on mechanical behavior of steels, not precipitation hardening alloy in particular, and concluded that the strain-rate dependence at high temperature could have an important contribution to the mechanical behavior during continuous casting. Pierer et al. (2005) used the data provided by Kozlowski et al. (1992) for the Ramberg-Osgood and Norton's law for ST 52 steel.

3.3 Task Breakdown

The proposal original budget for the DOE funds was $K 370, while only $K 189 were received. Accordingly, the proposal original budget for the in-kind funds was reduced from $K 567 to $K 349. Thus, the original scope of the project had to be narrowed.

Table 3.1 Proposed and actual budget.

FY	04	05	06	07	Total
DOE funds (original) $K	32	169	169	-	370
DOE funds (actual) $K	32	63	67	27	189
In-kind funds (original) $K	49	259	259	-	567
In-kind funds (actual) $K	-	311	26	12	349

The tasks for this project were as follows:

Task 1: Design Die Molds For Wax Patterns
- 1.1 Select Part and Specify Design Requirements
- 1.2 Implement Design Requirements
- 1.3 Create Finite Element Meshes
- 1.4 Inject Wax Patterns.
- 1.5 Measure Wax Pattern Dimensions

Task 2: Obtain Properties of Filled Waxes and Determine Wax Shrinkage Allowance -
- 2.1 Measure Density and Thermal Expansion
- 2.2 Measure Thermal Conductivity and Specific Heat Capacity.
- 2.3 Measure Shear Modulus and Bulk Modulus

Task 3: Determine Shrinkage Allowance Due to Shell Molds-
- 3.1 Obtain Thermophysical Properties for the New Shell Materials.
- 3.2 Invest Shell Molds, Dewax Shell Molds, and Measure Shell Mold Dimensions

Task 4: Determine Alloy Shrinkage Allowance
- 4.1 Obtain Thermophysical and Thermomechanical Properties
- 4.2 Develop And Implement Constitutive Equations
- 4.3 Conduct Controlled Casting Experiments
- 4.4 Perform Numerical Simulations for Various Process Conditions

Task 5: Documentation and Technology Transfer
- 5.1 Write Reports on Shell, Wax, and Alloy Results and Approaches
- 5.2 Present results to professional meetings and review meetings

4. Results and Discussion

In this work, deformations shell-alloy systems were considered in a coupled manner, but the coupled deformation of the wax-shell system was not considered. Therefore, the project contained tasks pertaining to each material and their interactions, which are described in distinct sections. Section 4.1 presents results for the work on shell mold material. Section 4.2 describes results for the alloy and shell-alloy deformation, and Section 4.3 deals with the wax materials.

4.1 Shell Mold Properties

In this section, the data on properties of alumino-silicates materials used for shell molds are reviewed. In addition, a zircon and fused silica shell system was selected (Sabau and Viswanathan, 2004), and either three or five backup coats were used. Material property data, which were not available from material suppliers, was obtained. The experimental part of the program was conducted at ORNL and commercial foundries, where wax patterns were injected, molds were invested, and alloys were poured. Due to the budget restrictions, project was funded at approximately 50% of the proposed amount, no temperature data were obtained from actual castings. For fused silica molds, the shell deformation during the prefiring phase was neglected, since the fused silica has a very low thermal expansion property, approximately five times less than that of any other shell mold material, ensuring that shell deformation during the prefiring is minimal.

4.1.1 Material Property Data for Shell Molds

In this section, the data on properties of alumino-silicates are reviewed. For this project, the investment of the shell molds and casting was conducted at three foundries (Table 4.1).

Table 4.1. Shell systems used. The prime coat was zircon.

Company	*Backup coats*
PCC	Alumino-silicate
Viking Metalgraphics	Alumino-silicate
SeaCast	Fused Silica

The shell mold suppliers provided property data that was measured. As shown in Tables 4.2 and 4.3, some properties, which are needed for the numerical simulation of thermal and deformation phenomena, were not available from the suppliers.

Table 4.2. Thermophysical properties available from suppliers and property needed for numerical simulations.

Supplier	Material	Available-Thermophysical Properties	Needed - Thermophysical Properties
C-E Minerals	Mulcoa 47	Density, Porosity, Reheat Change (% vol)	specific heat, thermal conductivity
Remet	Remasil 48	Density, Porosity	specific heat, thermal conductivity
Ransom & Randolph	-	Density	specific heat, thermal conductivity
Minco	Fused silica	Yes	None

Table 4.3. Thermo-mechanical properties available from suppliers and property needed for numerical simulations

Supplier	Material	Available-Thermo-mechanical Properties	***Needed – Thermo-mechanical Properties
C-E Minerals	Mulcoa 47	None	Thermal expansion, Youngs modulus, Poisson ratio
Remet	Remasil 48	Coefficient of thermal expansion, Thermal expansion	Youngs modulus, Poisson ratio
Ransom & Randolph	-	none	Thermal expansion, Youngs modulus, Poisson ratio
Minco	Fused silica	Youngs modulus, (Snow, 2004)	Thermal expansion, Youngs modulus as a function of temperature, Poisson ratio

***For large parts, or for shell molds that are exposed to high temperatures for long times, the creep properties are needed also.

The following properties were provided by Remet for the Remasil 48 shell mold: Density (2.62 g/cc, Thermal expansion 5.3E-6 in./in./F, and Porosity (3.6).

A literature review was conducted on thermophysical properties alumino-silicates to find data on those properties that were not available from material suppliers (Table 4.3). It was found that the thermal conductivity was either constant, with values from 0.75 to 1 W/mK, or temperature dependent with increasing values. At high temperatures, such as those for the steel casting, the shell molds become semi-transparent, effect that can be thought of as an increase in thermal conductivity of the mold (for fused silica, Sabau and Viswanathan, 2004). This effect was not observed in the data shown in Table 4.4. This could be explained by the fact that Browne and Sayer (1995) and O'Mahoney and Browne (2000) investigated the properties of alumino-silicates for the investment casting of aluminum alloy, a relatively low temperature domain as compared to that for steel casting. The other studies were not performed for investment casting molds. Russell et al. (1987) obtained data for thermal conductivity, specific heat, and thermal expansion of mullite. Table 4.5 shows some data available for the heat transfer coefficients for alumino-silicates shell systems.

Achari and Satapathy (2003) showed data on Youngs modulus for mullite that was fabricated by isostatic pressing, extrusion, and ramming processes. A review of mechanical properties of alumino-silicates, including those of alumina, is presented in Table 4.6. Munro (2004) presented an analytical relationships for the temperature and porosity dependence of the elastic and bulk moduli of polycrystalline ceramics, which was applied for twenty four oxide ceramics, as:

$$E(T, \phi)=229\ (1-1.17\text{E-}4\ T)\ (1-\phi)^{3.33} \qquad (4.1)$$

$$G(T, \phi)=166\ (1-1.16\text{E-}4\ \ T)\ (1-\phi)^{3.15}, \qquad (4.2)$$

where E is the Youngs modulus, G, bulk modulus, ϕ, porosity, and T, temperature.

Table 4.4 Thermophysical properties reported for the investment casting shell molds.

Property	*Material*	*Values*	*Temperature (^oC)*	*Reference*
Emissivity	alumino-silicate	0.615	400 to 700	Browne and Sayer (1995)
Emissivity	alumina	0.8, 0.8, 0.4, 0.4	RT; 100; 1,100; 1,600	Touloukian (1972)
Thermal conductivity (W/mK)	alumino-silicate	1.0	400 to 700	Browne and Sayer (1995)
Thermal conductivity (W/mK)	molochite	0.6, 0.85, 0.78, 1.16	170, 210, 300, 325	Browne and Sayer (1995)
Thermal conductivity (W/mK)	molochite	0.75	400 to 700	O'Mahoney and Browne (2000)
Thermal conductivity (W/mK)	mullite	2.1, 1.4, 1.2, 1.1, 1.0, and 0.8	RT, 300, 400, 500, 700, and 1,500	Russell et al. (1987)
Specific heat (J/gK)	alumino-silicate	0.8	400 to 700	Browne and Sayer (1995)
Specific heat (J/gK)	molochite	1.02, 1.14	300, 700	O'Mahoney and Browne (2000)
Specific heat (J/gK)	mullite	0.13901*ln(T[C])+ 0.28668	RT to 1,400 C	Goodson (1997)

Table 4.5. Heat transfer coefficient at metal-mold interface

(obtained for Inconel 718 alloy by Sahai and Overfelt, 2000)

HTC W/m^2K	Metal Temperature ^oC	Casting Configuration
200	1,300	cylinder
100	850	cylinder
5,000	1,400	plate
100	1,100	plate

Table 4.6. Mechanical properties reported in the literature for alumino-silicates.

Property	*Material*	*Value*	*Variables, Temperature (^oC)*	*Reference*
E, creep rate	Sintered, porous alumina		RT, 1100 Porosity	Hammond and Elzey (2004)
E (GPa), Poisson ratio, creep rate	Sintered Alumina	E=417-0.0525*T		Munro (1997)
G (GPa)	Sintered Alumina	$G=252*(1-\phi)^5$	Porosity	Munro (2001)
E (GPa) (green shell)	molochite	1-3; 3-6	Shell thickness, z<3.5mm; z > 3.5mm	Jones et al. (2002)
Creep rate	Fused silica		400 to 700	Wereszczak et al. (2002)
E (GPa); G (GPa)	mullite	Eq. 4.1 and 4.2	Temperature; RT to 900; porosity	Munro (2004)

4.1.2 Material Property Data for Fused-silica Shell Molds

The thermal expansion of the shell mold was available from Snow (1995). The shell material shows extremely small thermal expansion on heating (Figure 4.1). Sintering is evidenced by a change from expansion to contraction at approximately 900 ^{o}C. The data were obtained by holding the shell mold for 2 hours at 1200 ^{o}C. During cooling, the thermal contraction of the shell is larger than the expansion for heating, reaching 0.3 % at 200 ^{o}C. Due to crystoballite formation, the thermal contraction occurs at a different rate from 200 ^{o}C to room temperature. The thermal expansion of the shell mold is still much smaller than the thermal expansion of the alloy. Since insignificant thermal expansion occurs during heating, the dimensions of the shell mold do not change from room temperature until the metal is poured. This distinct behavior during heating and cooling of the fused silica shell molds is very important since the shell dimensional changes prior to metal pouring can be neglected. For alumino-silicate molds, this is not the case since their thermal expansion is significantly larger than that of the fused silica molds. Moreover, since the shell is much less stiff than the steel, its contraction behavior below 1200 ^{o}C is expected to alter the gap between the mold and casting while inducing insignificant deformation in the steel casting.

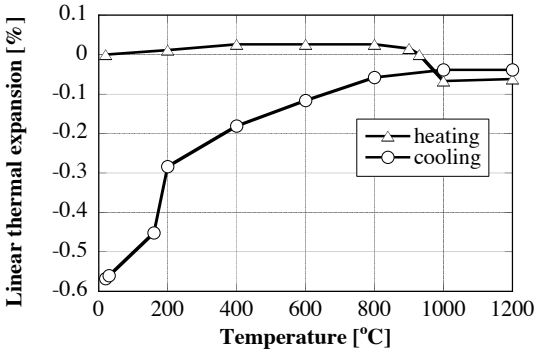

Figure 4.1. Measured linear thermal expansion for the shell mold (Snow, 1995).

The shell mold contained the following types of substrates: face coats, intermediate coats, backup coats, and seal coats. Each coat was generally made of two layers, a slurry layer and a stucco layer. In this study, zircon and fused silica shell materials were used (Sabau and Viswanathan, 2004). The shell mold had eight coats: a zircon prime coat, one intermediate coat, five backup coats, and one seal coat. The shell mold thickness was approximately 8.5 mm.

In order to account for thermal radiation effects within the shell mold, the following relationship proposed by Sabau and Viswanathan, (2004) for temperature dependence of thermal conductivity, k, was used:

$$k(T) = a_k + b_k T^3. \qquad (4.3)$$

For a shell mold with a thickness of approximately 8.5mm, parameters a_k and b_k were found to be 0.48 and 3.61 10^{-10}, respectively (Sabau, 2005). The shell mold was considered to be a linear-elastic material, for which the Young's modulus at 25 ^{o}C was approximately 2,586 MPa (Snow, 2004). The temperature dependence of Young's modulus was that provided by Fukuhara and Sanpei (1994) and Munro (2004) for fused silica.

4.2 Alloy Properties and Mechanical Interaction for the Shell-Alloy System

In this section, the first attempt to determine shrinkage factors for the investment casting of stainless steels is presented. For all the properties of 17-4PH stainless steel, the experimental data available in the literature did not cover the entire temperature range necessary for process simulation. Thus, some material properties were evaluated using ProCAST, based on CompuTherm database. A comparison between the predicted material property data and measured property data was made. It was found that most material properties were accurately predicted only over several temperature ranges. No experimental data for plastic modulus were found. Thus, several assumptions were made and ProCAST recommendations were followed in order to obtain a complete set of mechanical property data at high temperatures. Thermal expansion measurements for the 17-4PH alloy were conducted during heating and cooling. As a function of temperature, the thermal expansion for both the alloy and shell mold materials showed different evolution on heating and cooling.

Section 4.2 is concerned with determining the alloy tooling allowances from a combined analysis of heat transfer and deformation of the casting process. The shell molds were made of fused silica with a zircon prime coat, as shown in previous sections. The wax patterns were invested at Minco, Inc., and casting experiments were conducted at Precision Metalsmiths, Inc. (PMI). Dimensions of the die tooling, wax pattern, and casting were measured using a Coordinate Measurement Machine. Numerical simulations were performed using ProCAST for the investment casting of 17-4PH stainless steel parts in fused silica molds using the thermal expansion obtained on heating and another one with thermal expansion obtained on cooling. Since the fused silica shells had the lowest thermal expansion properties in the industry, the dewaxing phase, including the coupling between wax-shell systems, was neglected. The shell mold was considered to be a pure elastic material. The alloy dimensions were obtained from numerical simulations. For 17-4PH stainless steel parts, the alloy shrinkage factors were over-predicted, as compared with experimental data.

4.2.1 Thermophysical Material Property for 17-4PH steel

The first step in predicting alloy shrinkage factors was to obtain data on thermophysical properties of 17-4PH alloy. Experimental data on material properties were reviewed. Experimentally measured data on specific heat and thermal conductivity were provided in Fieldhouse and Lang (1961) for temperatures less than 1200 and 1395 ^{o}C, respectively. Experimental data on density and thermal expansion were available from measurements reported for heating by Touloukian et al. (1979) and Rack (1981) (up to 940 ^{o}C). No experimental data were available for the solidification properties, such as solidus, liquidus, and distribution of solid fraction. Thus, it was found that the material properties for 17-4PH alloy, which were required for the numerical simulations, were not available over the entire temperature domain experienced in the process (from the liquidus to room temperature). In order to obtain the material property data at high temperatures, computational techniques were reviewed. Recent advances in thermodynamics and material science were exploited to obtain data on material properties (Guo and Samonds, 2007). For example, the CompuTherm database (Chen et al., 2003) for molar volume and thermal volume coefficients of expansion (CTE) of liquid, solid solution elements, and intermetallic phases, was used to estimate the densities of the liquid and solid phases (Guo and Samonds, 2007). However, these methods have not been validated for stainless steel alloys, such as 17-4PH. Next, CompuTherm software available with ProCAST^{TM} was used to obtain the data on specific heat (Figure 4.2a), enthalpy, latent heat, electrical conductivity and resistivity, thermal conductivity (Figure 4.2b), solid fraction (Figure 4.2c), density (Figure 4.2d), and liquid viscosity. Where available, the experimental data are also shown in Figure 4.2. The composition, % wt, that used in CompuTherm simulations was Al 0.002, B 0.002, Cd 0.2, C 0.027, Cr 15.21, Co 0.05, Cu 3.47, Mn 0.63, Mo 0.1, Ni 4.44, N 0.02, P 0.028, Si 0.43, S 0.026, Ta 0.022, Ti 0.002, Fe balance. The estimated properties using ProCAST were compared against experimental data. It was found that the following properties were predicted with a high degree of accuracy:

specific heat, thermal conductivity (above about 750 °C), density and thermal expansion during heating.

Based on this good agreement between the experimental and estimated property data, a complete set of material property data was created by combining the experimental data that were available at low/moderate temperatures with estimated data at high temperatures. Table 4.7 shows which experimental and estimated data were used to create the material property data set for thermophysical properties. For example, the density data, which were used in the simulations, were created by shifting the estimated data such that they would be in good agreement with the experimental data (Figure 4.2d). For thermal conductivity, the estimated data below 700 ^{0}C were discarded.

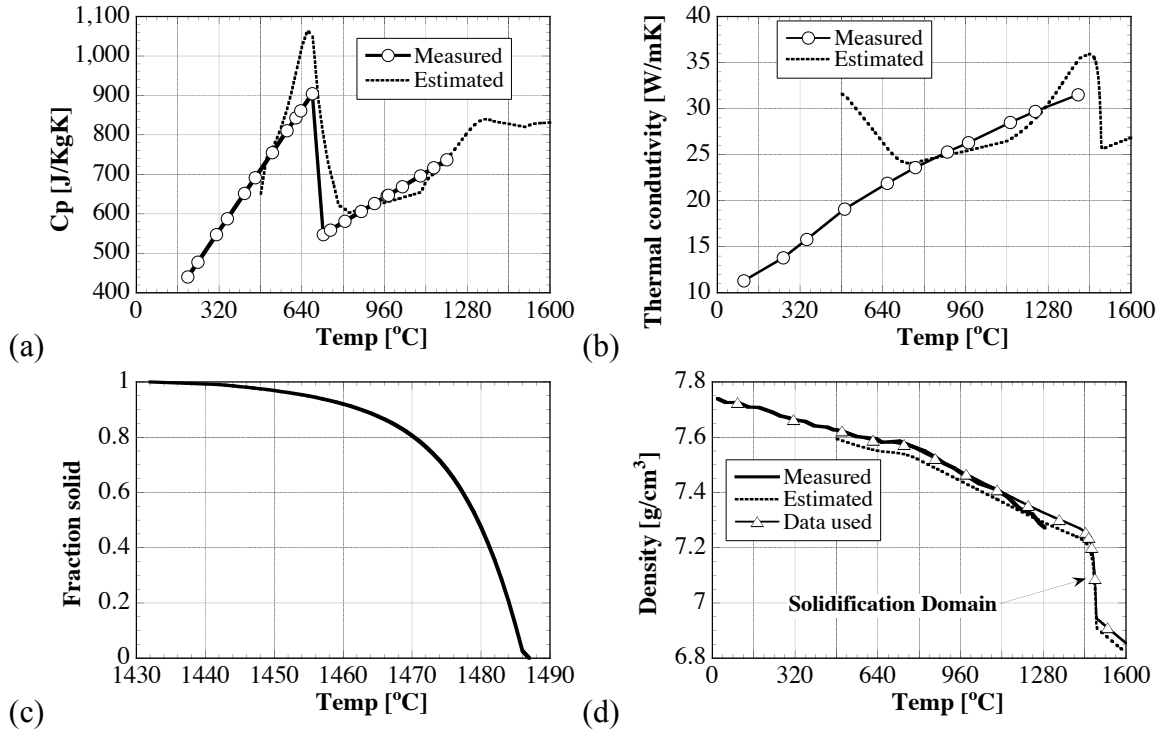

Figure 4.2. Thermophysical properties for 17-4PH alloy, (a) specific heat, (b) thermal conductivity, and (c) fraction solid, (d) density. Density was obtained from thermal expansion data on heating.

Table 4.7 References for Measured Data on Material Property.

Property	*Reference for measured data*	*Property used in numerical simulations*
Fraction solid	-	Estimated
Density (Thermal expansion)	Touloukian et al. (1979)	combined measured and estimated data
Specific heat	Fieldhouse and Lang (1961)	estimated
Thermal conductivity	Fieldhouse and Lang (1961)	combined measured and estimated data

Thermal contraction during cooling is a very important property for dimensional predictions. Since density and thermal expansion were available only on heating, thermal expansion measurements in the 20-1360 ^{o}C temperature range were carried out using a push rod dilatometer (Porter and Maziasz,

1993; Frankel et al., 2005). Three measurement runs were performed in flowing helium using heating and cooling rates of 3 °C/min. The experimental results show an excellent reproducibility (Figure 4.3a) for the three runs considered. The data show that the curves for heating and cooling do not follow the same behavior. During heating the 17-4PH alloy is primarily composed of a tempered martensite phase up to about 700 °C where this phase starts to transform to the austenite phase. This transformation is accompanied by both a volumetric contraction and a larger CTE for the austenite phase. Both of these effects are evident in the heating curve of Figure 4.3a. During cooling, at approximately 265 ^{o}C, the alloy shows an abrupt expansion (rather than continued contraction). This expansion is brought about by the transformation of the high temperature austenite phase back to martensite. The exact temperature for the start of this transformation, M_s, is determined by the chemical composition of the austenite. In the dilatometer runs of this study, conducted at cooling rates of 3 °C/min, carbides can precipitate below 800 °C which will change the austenite composition, thus raising M_s considerably above room temperature (Irvine et al., 1979). The overall thermal expansion/contraction on heating and cooling, from room temperature to high temperatures to room temperature, was about the same.

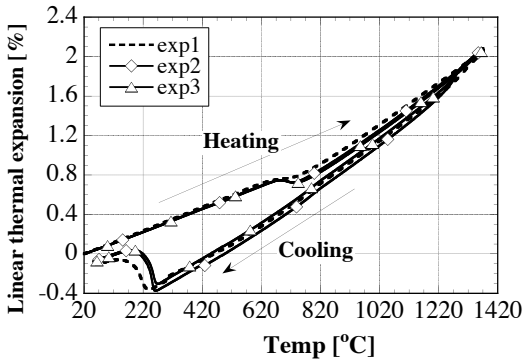

Figure 4.3. Measured linear thermal expansion for 17-4PH alloy on heating and cooling.

4.2.2 Thermomechanical Material Property for 17-4PH steel

The data on mechanical properties, which are needed for the numerical simulation of alloy deformation, were not readily available, especially at high temperatures. The experimental data available for the Young's modulus was limited to 900 ^{o}C. As with the thermophysical property data, the thermomechanical property data were measured and reported in several references at relatively low temperatures, i.e., $T < 0.5\ T_S$, where T_S=1,430 ^{o}C is the solidus temperature. A literature review was conducted on elasticity and plasticity properties for 17-4PH or 15-5PH (Table 4.8). Using the same methodology from Guo and Samonds (2007) the liquid viscosity, Young's modulus, and Poisson's ratio were estimated. The measured data and estimated data for Young's modulus are shown in Figure 4.4a. For temperatures between 700-900 ^{o}C, the estimated Young's modulus was in good agreement with experimental data. The ProCAST data at temperatures lower than 750 ^{o}C were excluded from the newly generated set of data for the Young's modulus. Figure 4.4b shows the data For Young's modulus only in the high temperature domain.

Table 4.8. Thermo-mechanical properties available from suppliers and published references for 17-4PH or 15-5PH stainless steels.

Property	*Temperature range [^{o}C]*	*References/Notes*
Yield strength	20:400	Wu and Lin (2003)
Young's modulus	20:500	Sandmeyer (2005)
0.2%YS, Elongation %	540:1090	AK Steel, 17-4PH data
Young's modulus	20 : 315	AK Steel, 15-5PH data
Yield strength	20:540	ASM alloy Center: Materials Property Data
Stress strain curves, Ramberg-Osgood	25:480	MMPDS, 15-5PH data, compression
Stress strain curves	950:1250	Atlas of Formability (ABAQUS format)

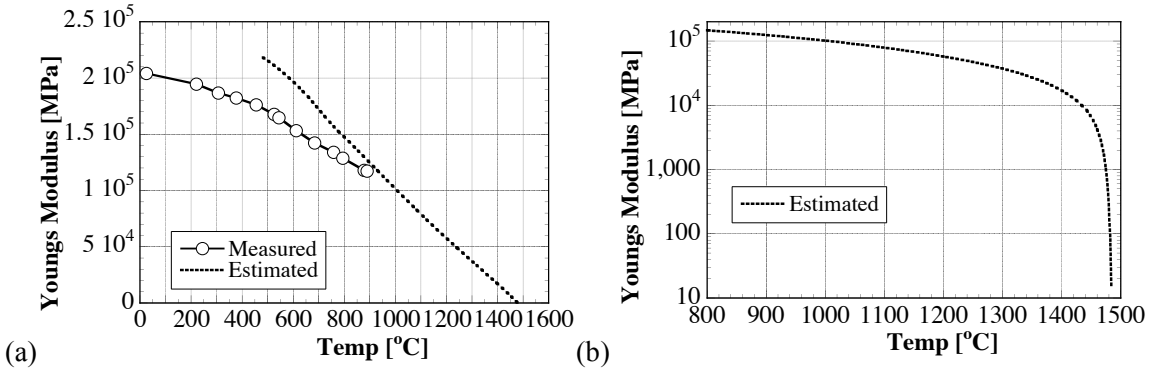

Figure 4.4. Modulus of elasticity for 17-4PH alloy (Experimental data from Rack, 1981) (a) over large temperature domain, (b) at high temperature.

One important parameter that describes the plasticity behavior is the yield stress. The data on plasticity for these alloys are scarce and do not include the entire temperature domain (Table 4.8). The yield strength, which was estimated from data found in the Appendix A, is shown in Table 4.9. The ASM Alloy Center published data at a temperature range of 25 to 650 ^{o}C (Table 4.9). The data for yield strength near the solidus were not available and ProCAST recommendations were followed for setting the yield strength at those high temperatures. In summary, Table 4.9 shows the yield strength used for simulations was obtained by taking into account the data set from ASM, Atlas of formability, and ProCAST recommendations. In the simulations, a linear temperature variation between consecutive data points was assumed.

Several advanced models for the numerical simulation of stress, strain, and the ensuing displacement fields during casting have been developed in academia over the last decade (Bellet et al., 1996, Drezet and Rappaz, 1996). These models were recently implemented in commercial simulation software ProCAST^{TM}. According to the small strain theory, the total strain can be decomposed into strain components that correspond to the elastic, viscoplastic, thermal, and liquid-solid phase transformation effects. The elastic strain was related to the internal stresses by Hook's law. For aluminum alloys, Bellet et al. (1996) developed a methodology for modeling casting solidification by including constitutive equations for the mushy zone and liquid regions into a solid model that is based on Perzyna (1963).

Table 4.9. Yield stress as a function of temperature.

Temp. [^oC]	*[X]Estimated (AOF)*	*ASM Alloy Center*	*Data used in this study*
25		1158	1158
204		958	958
315		931	931
371		903	903
427		889	889
482		814	814
538		696	696
650		283*	283
950	104 to 85		104
1000	45		
1050	35		
1100	25		
1150	17		
1200	9		
1250	7		
1432**			17.375
1487***			5.21

*Data for 15-5PH

[X]Estimated from Atlas of Formability (AOF) data

**solidus point, yield strength for H13 steel available in ProCAST

***liquidus point, yield strength above 5 MPa for fs < 50% (ProCAST recommendations)

The stress module was coupled with the fluid flow module in ProCAST, such that appropriate constitutive equations were available for the liquid, semi-solid, and solid states that coexist during casting solidification. The elasto-plastic model based on the linear hardening law is defined as:

$$\sigma_Y = \sigma_o + H\varepsilon^{pl} \ , \qquad (4.4)$$

where σ_o = the yield stress, ε^{pl} = the plastic strain, and H = the plastic modulus, and σ_Y = the modified yield stress due to linear hardening. Depending on the amount of solid fraction, deformation and/or fluid flow phenomena take place. The transition from fluid dynamics to solid dynamics was considered to take place at a certain solid fraction. Since no experimental data were available for the critical solid fractions for thermomechanical behavior of 17-4PH, the fluid-solid dynamics transition was considered to occur at the solid fraction of 0.90, which was found to be appropriate for the numerical simulation of shrinkage deformation of A356 aluminum alloy (Sabau, 2006).

Plastic models with isotropic hardening are used in continuous casting modeling due to their easy computational implementation. A more complex treatment for thermo-mechanical behavior is the viscoplastic model, in which the strain rate dependence is considered. Fachinotti and Cardona (2003) reviewed data on mechanical behavior of steels, not precipitation hardening alloy in particular, and concluded that the strain-rate dependence at high temperature could have an important contribution to the mechanical behavior during continuous casting. The viscoplastic behavior is described by the following equation:

$$\dot{\varepsilon}^{pl} = \frac{1}{\eta}\left\langle |\sigma| - \sigma_Y \right\rangle^n \frac{\sigma}{|\sigma|}, \qquad (4.5)$$

where σ is the applied stress, n is the power exponent, η is a viscous parameter. The operator $< . >$ is defined as $< f > = f$ when $f \geq 0$ and zero otherwise. Both n and η are temperature dependent coefficients. For example, at low temperatures when the alloy tends to behave elastoplastic, n has very large values while η has very small values. The plasticity property data did not cover the entire temperature range needed and the data for plastic modulus were especially difficult to find.
The only data available to estimate n and η parameters were the true-stress true-strain data from the Atlas of Formability. The limited temperature range for the Atlas of Formability data hinders the use of this data, as data at low temperatures and near the solidus are not available. Other options would be to use viscoplastic data that were obtained for other steels (Table 4.10). Pierer et al. (2005) used the data provided by Kozlowski et al. (1992) for the Ramberg-Osgood and Norton's law for ST 52 steel. Thus, for isotropic linear hardening, ProCAST recommends the use of a fraction of the Young's modulus, i.e., H=E/20.

Table 4.10 Mechanical properties for other steels than 17-4PH.

Property	*Material*	*Equation, Property*	*Temperature Range (^oC)*	*Reference*
E, $Y_{0.2}$	Stainless steel (304)	Ramberg-Osgood, stress-strain model	RT	Abdella (2006)
E, $Y_{0.2}$, $Y_{0.5}$, $Y_{1.5}$, $Y_{2.0}$	EN 1.4462, AISI 304	stress strain model	RT to 960	Chen and Young (2006)
Creep rate	Continuous casting steel	Creep law, stress-strain model	Below solidus	Kajitani et al. (2001)
Creep rate	Austenitic steels	Norton's law	Below solidus	Kozlowski et al. (1992)
E, creep rate	Low carbon steels	Viscoplasticity, hardening	Below solidus	Fachinotti and Cardona (2003)

E – Young's modulus, Y_X – Yield strength at x% of strain, T – temperature

4.2.3 Experimental Results for Alloy Shrinkage Factors

Parts with six steps were examined in this study (Figure 4.5). The 2.54-cm-thick step is considered to be Step 1. Two types of stepped parts were made: parts without holes and parts with holes on steps 3 and 5. In the remainder of this study, alloy castings and wax patterns are simply referred to as parts and patterns. The patterns without holes and patterns with two holes are referred to as *no-hole, or unrestrained,* patterns and *two-hole, or restrained,* patterns, respectively. The two-hole patterns were made by placing cores in the die. The two cores provided geometrical restraint on the length dimension of the part. For this work, wax patterns were made at M. Argueso & Co by injection of liquid unfilled wax, Cerita™ 29-51, at a pressure of 1.7 MPa (250 psi), at 65°C (150°F), with a dwell time of 120 s.

The casting configuration considered in this study contains a downsprue, a runner, and one casting (Fig. 4.6). The sprue was dimensioned such that there was enough metallostatic head to fill the entire part. The height of the downsprue and pouring cup is 17cm and 6.35cm, respectively. The section dimensions for the pouring cup were 6.35 × 6.35, 2.54 × 2.54, and 2.54 × 1.9 cm at the top of pouring cup, end of pouring cup, and end of sprue, respectively. The molds were preheated at temperatures of 1000°C (1830 °F) for 45 min.

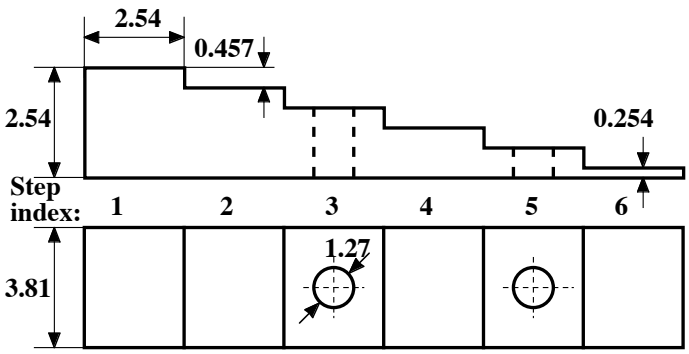

Figure 4.5: Wax pattern dimensions [cm] and step index.

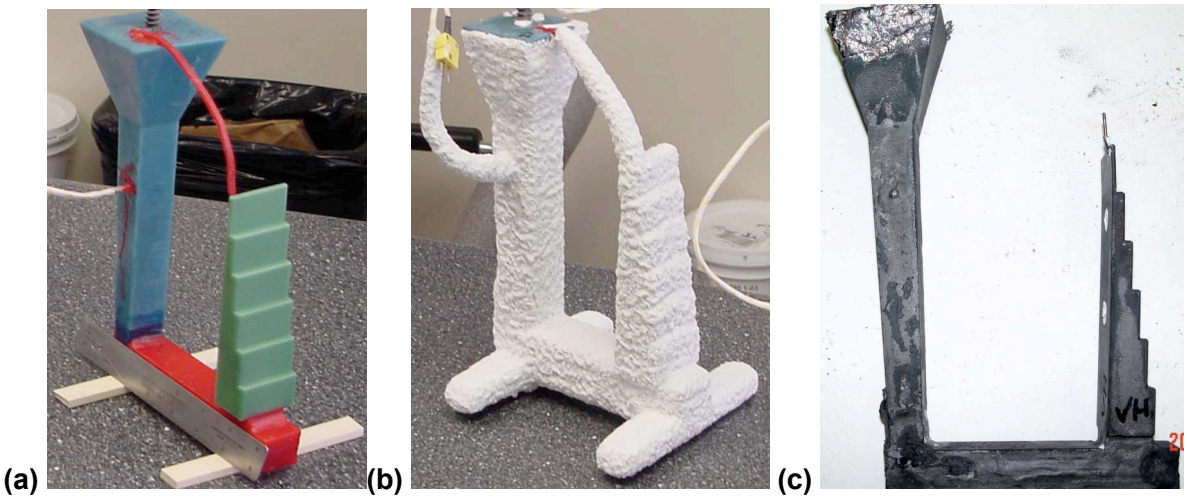

Fig. 4.6. Shell molds invested at Minco and cast at PMI: (*a*) wax pattern; (*b*) shell mold; (*c*) steel casting.

Dimensions of the die tool, wax patterns, and casting were measured at the same locations using a Coordinate Measurement Machine (CMM). CMMs are widely used throughout manufacturing industries to meet the high quality standards and dimensional accuracy. The probe size of the CMM was 3 mm diameter. The probe tips were round to within 0.0005 mm and the diameters were within 0.003 mm of nominal diameter. The probe tip actual diameter was calibrated against a reference sphere with a roundness uncertainty of plus or minus 0.0001 mm and a diameter uncertainty of 0.0002 mm. The measurement precision was plus or minus 0.02 mm.

Wax pattern dimensions were measured to provide a base line for casting dimensions. The wax patterns were examined under magnification to insure that no deformation was present in the surfaces after probing. The position of CMM measurement points are shown in Figure 4.7. The width shrinkage was calculated from the width coordinates for each pair of points, which were located at the same length and height but situated at opposite sides of the pattern. A representative length dimension was chosen to be *L2_5*, between the ends of Steps 2 and 5. Four no-hole patterns and four two-hole patterns were injected. Since the wax pattern showed good reproducibility, only two castings were made for each case. The parts were labeled as shown in Table 4.11.

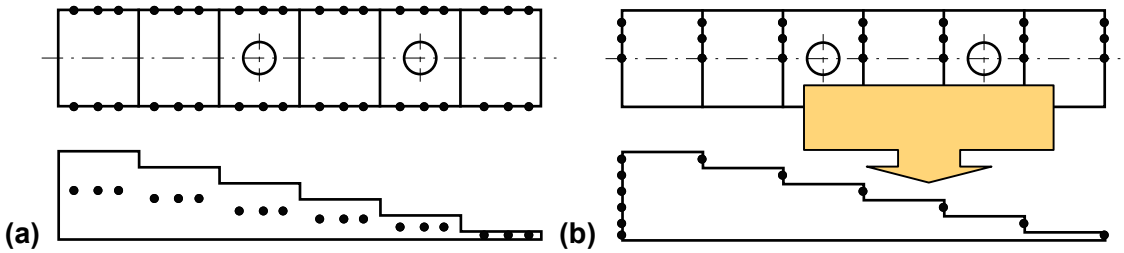

Fig. 4.7. The position of coordinate measurement points for (*a*) the width dimensions and (*b*) length L2–5, between ends of Steps 2 and 5.

Table 4.11. Index of wax patterns and castings

Part index	No. of holes in part	Part no.
0b1	—	1
0b2	—	2
2b1	2	1
*2b2	2	2

*The last step in the casting was incompletely filled and dimensions were not measured

The dimensional variations for the casting were calculated using the following relationship:

$$\text{Casting shrinkage } (c_s) = \frac{\textit{Pattern dimensions}}{} - \text{Casting Dimensions} \qquad (4.6)$$

The percentage of the shrinkage was calculated for the width dimension and length dimension (Figures 4.8). The width shrinkage was almost the same for cases 2b1 and 0b2. Part 0b1 showed lower shrinkage factors for steps 3, 4, 5, and 6, than the other two parts. For the *L2_5* dimension, the points with a zero width coordinate were located on the symmetry plane of the patterns, or centerline. The shrinkage was minimal at the centerline and largest at the edges. Smaller length shrinkage was measured for the restrained pattern, case 2b1. As indicated in Figure 4.8b for the case of overall casting shrinkage, the unrestrained parts shrink more than the restrained ones. The following general observations can be made concerning the dimensional measurements: (a) the width shrinkage factors were almost uniform, (b) the length shrinkage factors were larger at the edges than at the centerline, (c) the dimension, *L2_5*, for the two-hole restrained part showed smaller shrinkage than the unrestrained part.

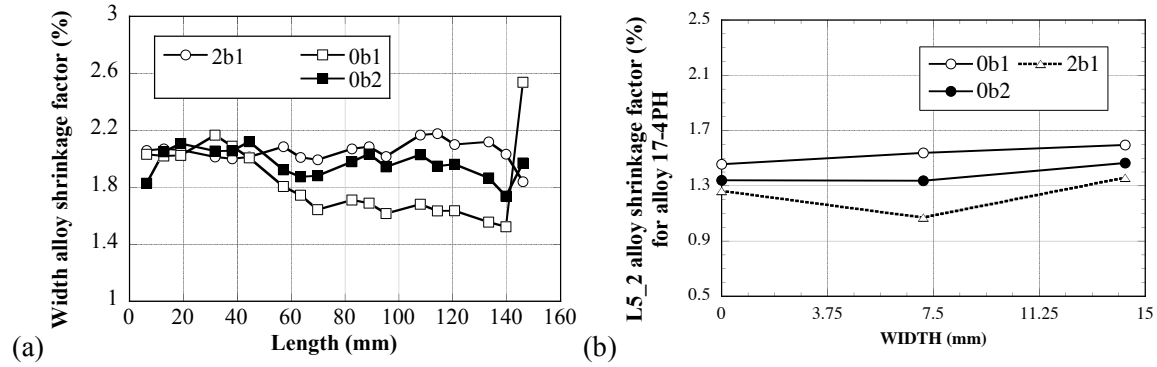

Figure 4.8: Alloy shrinkage factors for the (a) width dimension and (b) length dimension, L2-5.

4.2.4 Numerical Simulation Results for Casting Dimensions

Numerical simulations of heat transfer, solidification, and deformation during casting and subsequent cooling were conducted with ProCAST (Waite and Samonds, 1990) using the casting parameters, material properties, and boundary conditions given in the previous sections and Sabau (2005). The mesh was created using the shelling feature in MeshCAST, a module of ProCAST (Fig. 4.9). One mesh layer of 0.66 mm (0.026 in.) was used for the zircon face coat and another layer of 0.9 mm (0.036 in.) for the intermediate fused silica coat. Three layers of 1.2 mm (0.048 in.) each were used to model the fused silica back-up coats.

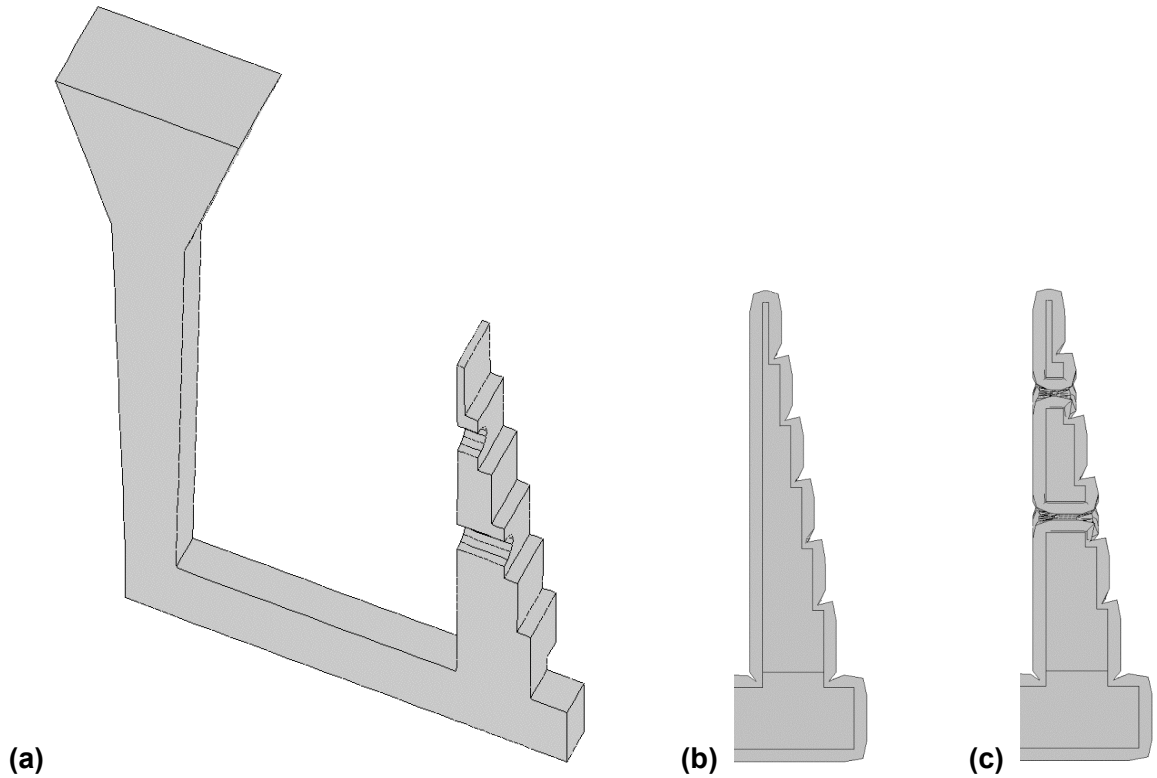

Fig. 4.9. Casting configuration for numerical simulations: (*a*) alloy material, and shell mold around the part; (*b*) part without cores, having unrestrained deformation; (*c*) part with cores, with length and width dimensions are partially constrained by cores.

The heat transfer coefficients (HTC) for this study were those used in Sabau (2005) and Sabau (2006). For the casting configuration in this study, the support structure was attached directly to the wax pattern. The mold support was invested [Figure 4.6(a)], allowing a more uniform cooling around the stepped pattern. HTC for the mold-air interface around the part, sprue, and runner were assumed to be 17, 38, and 7.5 W/m^2 K, respectively, while HTC for the metal surface at the top sprue, bottom surface of the mold in contact with the sand, and metal-mold interface were assumed to be 30, 42, and 850 W/m^2 K, respectively.

In addition to material parameters, there were software parameters that were used in the discretization of the stress-strain equations. These numerical parameters were introduced to increase the convergence rate or even to attain convergence. Preliminary simulations show that, due to the larger thermal contraction to room temperature, the steel casting deforms more than the aluminum alloys, requiring very robust solvers for the stress-strain equations. In Figure 4.10a, the evolution of the computed fraction solid in the center of the steps is shown. The part solidifies in approximately 2 min from the onset of pouring. The computed cooling curves are shown in Figures 4.10b and 4.10c for times of 0-30, and 30-90 min, respectively.

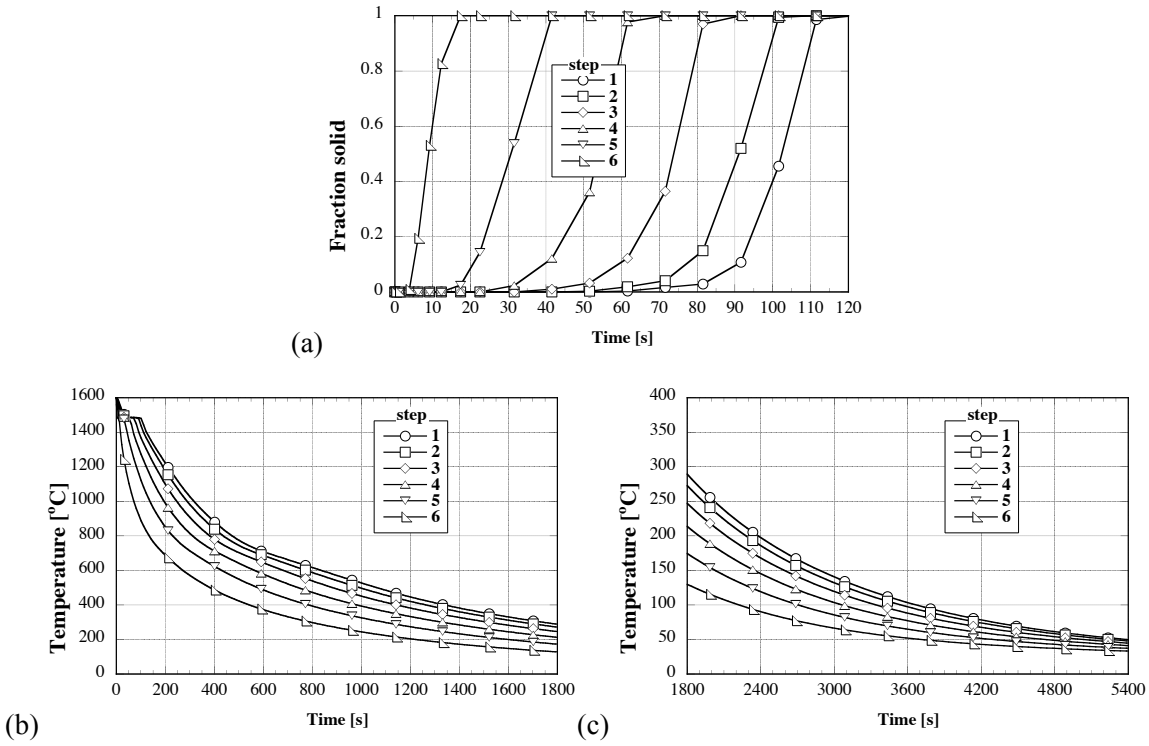

Figure 4.10: Evolution of the calculated solid fraction and temperature in the center of the steps (a) solid fraction (b) temperature (time < 1,800 s), and (c) temperature at longer times.

Most numerical simulations presented in other studies use thermal expansion data from heating measurements. As emphasized in the section on thermophysical properties, due to the distinct evolution of the thermal expansion of the alloy/shell during heating and cooling, two generic simulations were carried out, one with thermal expansion data obtained on heating and the other one with thermal expansion data obtained during cooling. The results obtained with these two options

will be referred in figures to as "heating" (or α_{heat}) and "cooling" (or α_{cool}). The results obtained with α_{heat} and α_{cool} will be compared.

The evolution of the calculated shrinkage factor, for the L2_5 dimension at the part centerline, is shown in Figure 4.11. There was an abrupt variation of the shrinkage in the first 300 s, as it increased to 1.5 and 0.9% for the no-hole and two-hole patterns, respectively. This shrinkage was approximately ¾ of the entire shrinkage computed at a time of 5,400s (90 min) from the onset of pouring. By looking at Figures 9 and 10, the abrupt shrinkage variation was found to occur when the temperature in the part was above 1,000 ^{0}C. The shrinkage evolution diverges for the α_{heat} and α_{cool} cases, shortly after the initial abrupt variation. At longer times, at approximately 3,000s, the results for the α_{cool} case come close to those of the α_{heat} case. Then, the cooling shrinkage shows a slow winding variation due to the passing of different regions in the casting through the martensitic domain at temperatures below 260 ^{0}C. For the two-hole pattern, the difference between the α_{heat} and α_{cool} cases is more evident at longer times (around 90 min), when the temperature in entire casting was below 85 ^{0}C.

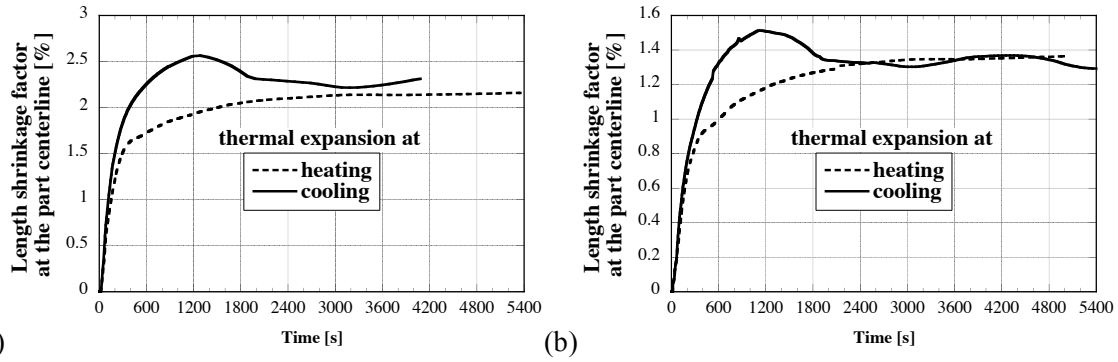

Figure 4.11: Evolution of the calculated shrinkage the L5_2 dimension at the centerline for the (a) no-hole pattern, (b) two-hole pattern.

The evolution of the shrinkage factor for the width dimension is shown in Figure 4.12 at the center of steps 2, 4, and 6. For these steps, the width dimension should exhibit approximately similar amounts of shrinkage, since along this dimension there are no mold features that provide the geometrical restraint. For the no-hole patterns (Figures 4.12a and 4.12b), the width shrinkage evolves asymptotically for the α_{heat} while for the α_{cool} case the shrinkage raises to higher values and then drops to those of the α_{heat} case. The same value is attained at longer times for all the steps considered. This is expected for unrestrained dimensions, as the overall thermal expansion for α_{heat} while for the α_{cool} cases is the same. Similar behavior is shown for the two-hole patterns (Figures 4.12c and 4.12d) as for the no-hole patterns, with the exception of the shrinkage for step 6. The shrinkage fraction in step 6 is less than that in the other steps. As will be seen later, this is due to the proximity of step 6 to the hole in step 5, which deforms much more than that in step 3, affecting the shape of the casting.

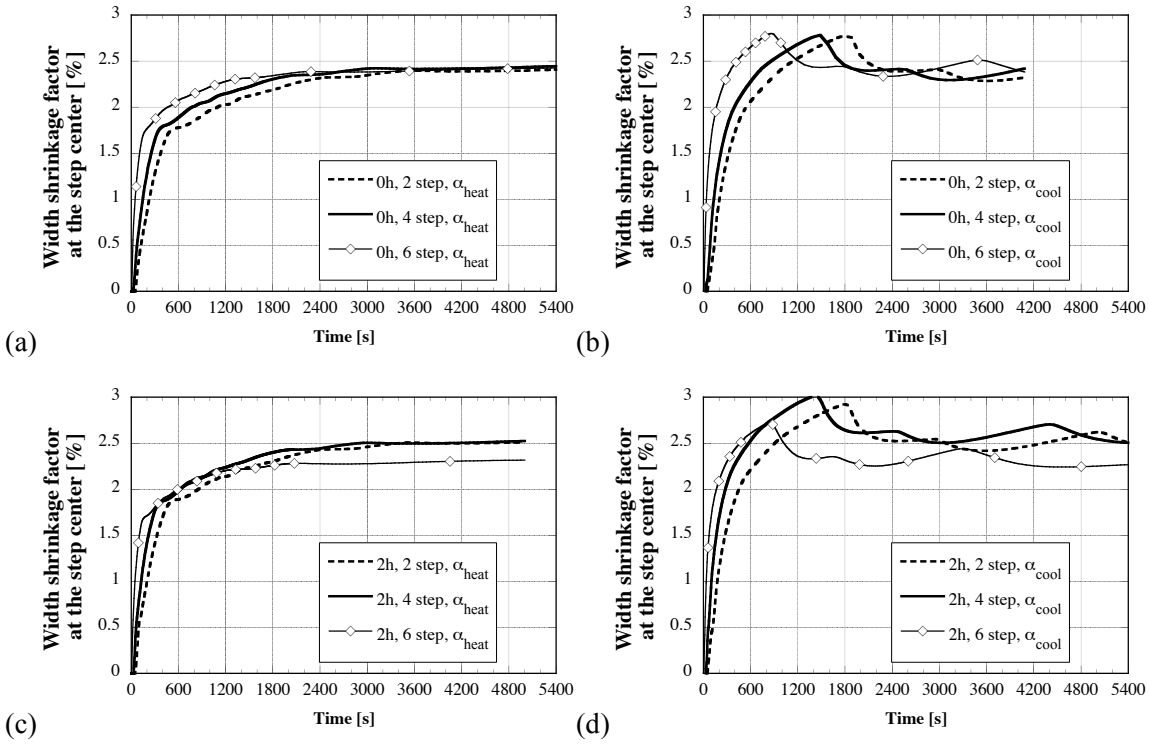

Figure 4.12: Evolution of the shrinkage the width dimension at the center of steps 2, 4, and 6 for the (a, b) no-hole pattern and (c, d) two-hole pattern. Thermal expansion of heating and cooling was used for results shown in (a, c) and (b,d), respectively.

The numerical simulation results are compared to experimental final shrinkage factors when the maximum temperature in part dropped below 85 ^{0}C, which was attained approximately 80-90 min from the onset of pouring. The comparison of the alloy shrinkage is shown in Figures 4.13 and 4.14 for the length and width dimensions, respectively. The measured dimensions were grouped according to the level of mold constraints. The unrestrained dimension groups include the length *L2_5* for the no-hole pattern, and width, *W*, for the no-hole pattern and two-hole pattern. The length *L2_5* for the two-hole pattern was restrained by the shell mold. The shrinkage factors for both unrestrained and restrained dimensions were slightly over-predicted. Nonetheless, with the exception of the L2_5 results for the no-hole part, the predicted shrinkage values are close enough to the measured values to allow a quantitative prediction of the shrinkage factors. The numerical results were very close for the α_{heat} and α_{cool} cases, with more differences for the width dimension (steps 5 and 6, distances of 90 to 140 mm in Figure 4.14b). It is likely that these differences may be amplified for more complex parts. There was no obvious reason for the shrinkage over-prediction. The over-prediction of shrinkage values could be due to assumptions used in the mechanical properties, especially at high temperatures, where most of the shrinkage occurred (Figure 4.11 and 4.12). For example, no experimental data for plastic modulus was found and ProCAST recommendations were followed to set its values. In order to find the reason for over-prediction, more experimental properties data are needed and a sensitivity study on plasticity properties needs to be performed.

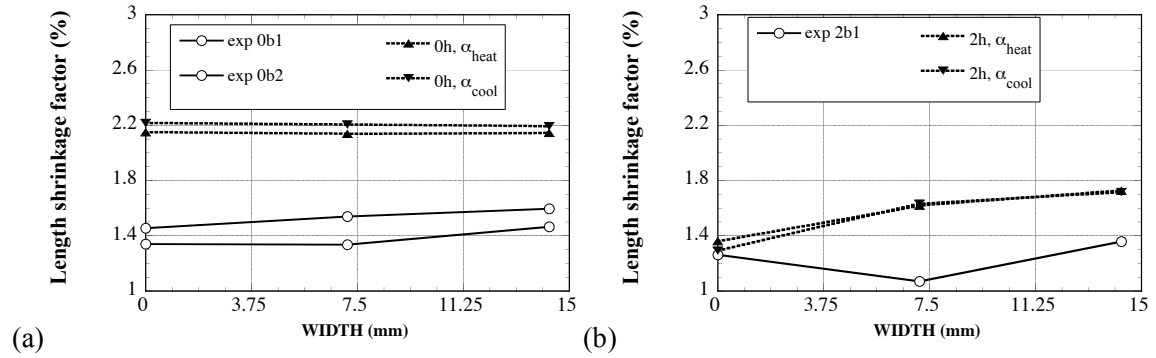

Figure 4.13: Comparison between the experimental results and computed results for the length dimension, L5_2: (a) part with no-holes and (b) part with two-holes.

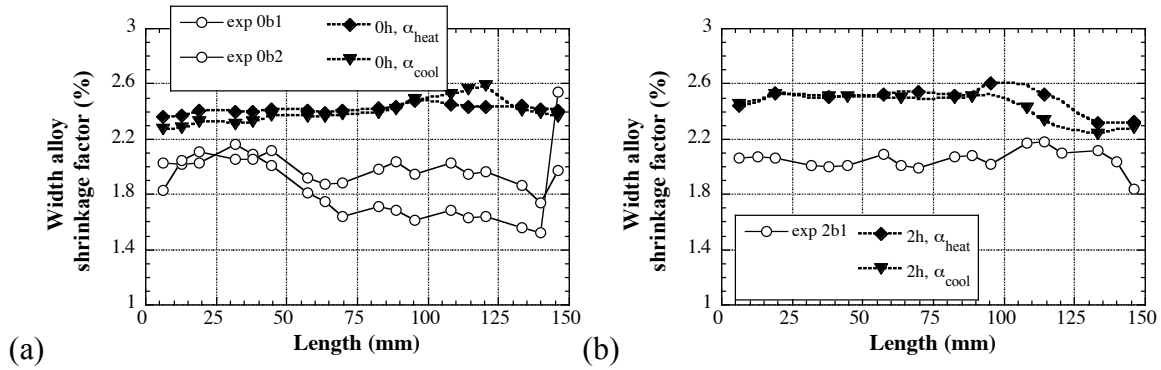

Figure 4.14: Comparison between experimental and computed shrinkage factors for the width dimension along the length: (a) part with no-holes and (b) part with two-holes.

The casting distortion was obtained from the numerical simulation results. Information on casting distortion can be used by engineers to visualize the distribution of the deformation. The deformation results shown in Figure 4.15 were obtained at a time of 4,080 s for the α_{heat} case. The same scale was used for both figures. As shown in Figure 14b for the width dimension, the effect of the hole in step 5 results in a necking feature between steps 4 and 5 while step 5 and 6 are largest among all steps. It is important to assess the extent of plastic deformation, since the elastic deformation will be relieved. Figure 4.16 shows the distribution of the equivalent plastic strain for the no-hole pattern. The α_{heat} results show evidence of plastic deformation in the step corners. On the other hand, for α_{cool} case, in which more accurate properties were used for the thermal expansion of the alloy and shell mold, the plastic deformation in the step corners was removed, and as expected, no plastic deformation takes place in the part, the region with highest plastic strain being located at the end of the runner. Figure 4.17 shows the distribution of the equivalent plastic strain for the two-hole pattern. Significant plastic deformation is shown for the hole in step 5. As for the no-hole pattern, α_{heat} results shows evidence of plastic deformation in the step corners, plastic deformation that was removed for the α_{cool} case. The highest plastic strain was located for the two-hole part in the part and not at the end of the runner, as it was for the no-hole case. This was due to the geometry of the entire casting, including the runner system. The two-hole part was "anchored" in the runner and was pulled away from the two holes towards the bottom of the part, where thick regions solidified well after the thin steps six and five. As a result of the geometrical constraint, the two-hole part did not deform

freely in the lengthwise direction, its shrinkage was less than the no-hole part, and thus, the two-hole part was longer.

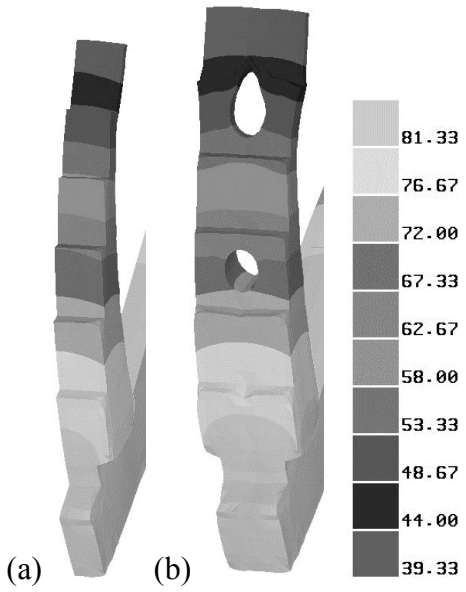

Figure 4.15: Temperature profile and part shape at 4,080 s. Thermal expansion from heating was used. (a) no-hole part, half of the part shown only, (b) two hole-casting.

Deformation was magnified 15 times.

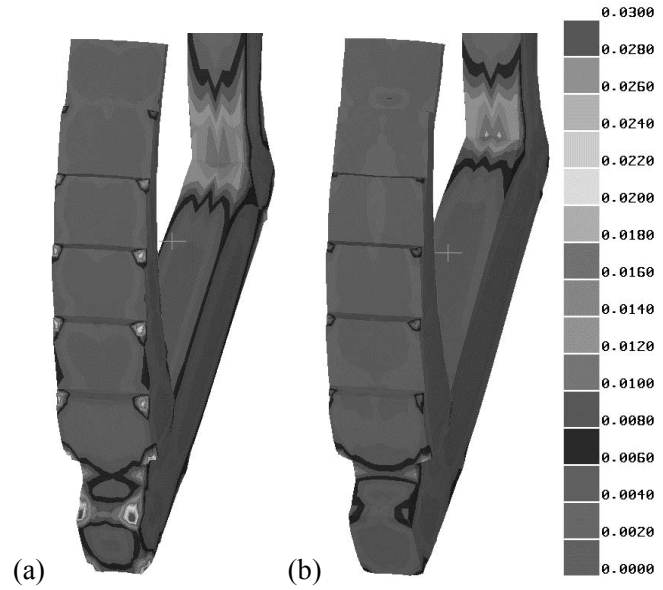

Figure 4.16: Equivalent plastic strain at 5,400s for the no-hole casting when thermal expansion used was that measured on (a) heating and (b) cooling.

Deformation was magnified 15 times.

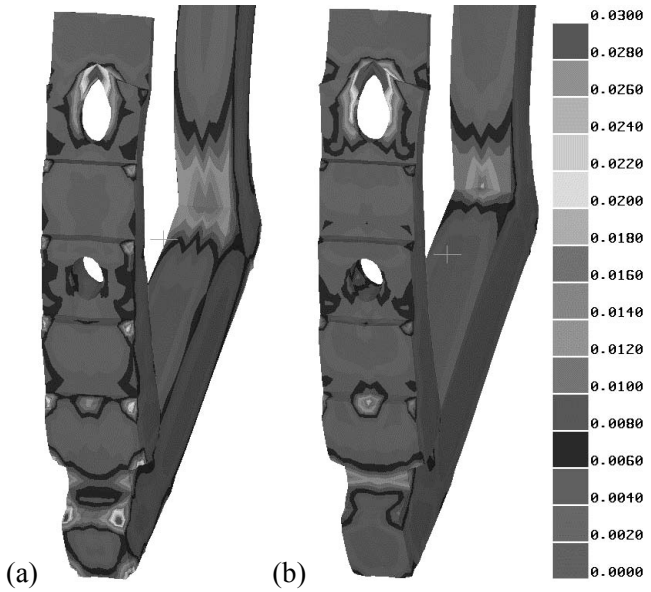

Figure 4.17: Equivalent plastic strain at 5,400s for the two-hole casting when thermal expansion used was that measured on (a) heating and (b) cooling. Deformation was magnified 15 times.

This study is the first attempt to determine shrinkage factors for the investment casting of stainless steels. The experimental data for 17-4PH stainless steel, did not cover the entire temperature range necessary for process simulation. Some property data had to be estimated using CompuTherm methodologies and recommendations from ProCAST. No experimental data for plastic modulus were found and ProCAST recommendations were followed to set its values. Numerical simulations were conducted to predict the alloy tooling allowances based on a combined analysis of heat transfer and deformation phenomena for 17-4PH stainless steel parts. Although the numerical results showed that the shrinkage evolution in time was quite different for the α_{heat} and α_{cool} cases, there was only a small difference in the final shrinkage factors predicted for these cases. The shrinkage factors were over-predicted for both the unrestrained dimensions and restrained dimensions. However, the effect of reduced shrinkage for restrained dimensions was adequately reproduced. With the exception of the L2_5 results for the no-hole part, the predicted shrinkage values are close enough to the measured values to allow a quantitative prediction of the shrinkage factors. The over-prediction of shrinkage values are likely due to assumptions used in the mechanical properties, especially at high temperatures, for which no experimental data were available. As expected, results showed that the plastic deformation occurred only in the two-hole casting.

4.3 Measurements of Material Properties for Filled Waxes

Additional R&D focus was placed on obtaining material property data for filled waxes, waxes that are common in the industry. The wax pattern dimensions are determined by the wax's thermophysical and thermomechanical properties, restraint of geometrical features by the metal die, and process parameters such as die temperature, platen temperature, injection pressure, injection temperature, and dwell time. In this report, material property data that is needed to determine dimensional changes associated with the wax system are provided.

The following waxes were chosen by participating companies for testing: Cerita F20-6, Cerita F20-844B, and Remet PR-15. For Cerita F20-6 wax, the filler was terepthalic acid, filler weight 42%, and filler volume of 31.6 %. The test bar mold was fabricated by Independent Tool, Inc. Test bars specimens of three waxes were injected at Schrey & Sons, Inc and McCaughin, Inc., commercial foundries. Rheometry measurement of filled waxes was conducted at ORNL. Material property measurements were conducted in this study for three filled waxes with the aim of obtaining a complete set of data that can be used as input in computer simulation software for predicting wax pattern dimensions. The measurement of viscoelastic properties of waxes is not a trivial task since the investment casting waxes are complex blend of polymers that exhibit a wide range of behaviors. The analysis of the rheometry data to obtain viscoelastic properties was not completed due to the reduction in the budget of the project (approximately 50% funds were received).

4.3.1 Thermophysical Properties of Waxes

In order to predict wax tooling allowances, all the properties that determine dimensional changes associated with wax processing must be evaluated. The Investment Casting Institute developed standard tests for the investment casting industry. For waxes, most of these tests are concerned with engineering properties, such as flow, softening point, strength, and sink. The available tests provide the information only for handling and processing wax patterns but are not useful for die design.

Data provided by the suppliers contains information on wax properties (Table 4.12), dimensional characteristics (Table 4.13), and operating conditions (Table 4.14). Aside from specific heat, which is necessary for thermal analysis, and thermal expansion property, none of the other data can be used to predict the shrinkage of complex investment casting patterns. Specific heat and thermal conductivity was measured for all the waxes considered (Figure 4.18). The results for the unfilled wax, Cerita^{TM} 29-51, were also reported in Figure 4.18 for comparison with the other filled waxes.

Table 4.12. Properties for the F20-6 wax provided by the wax supplier.

Property	Value
ring & ball softening point	159.5 ^{o}F / 70.8 ^{o}C
drop melt point	178.2 ^{o}F / 81.2 ^{o}C
hardness 450 grm. load	14.5 DMM
specific gravity	1.129
ash content (1800 ^{o}F/982c, 30 min)	0.0015%
filler content	42.0%
Viscosity	table data
Specific heat (and DSC data)	table data
Thermal expansion	table data

Table 4.13. Dimensional data.

Property	Value
step shrinkage in/in (mm/mm)	0.0060
step - cavitation in/face (mm/face)	0.0107/0.2718
10" linear shrinkage bar in/in (mm/mm)	0.0060

Table 4.14. Operating parameters

wax temperature	155 ^{o} F / 68.3 ^{o} C
nozzle temperature	157 ^{o} F / 69.4 ^{o} C
platen temperature	68 ^{o} F / 20 ^{o} C
pressure	300 psi/ 21 bar
flow control	30%
dwell time	60 sec

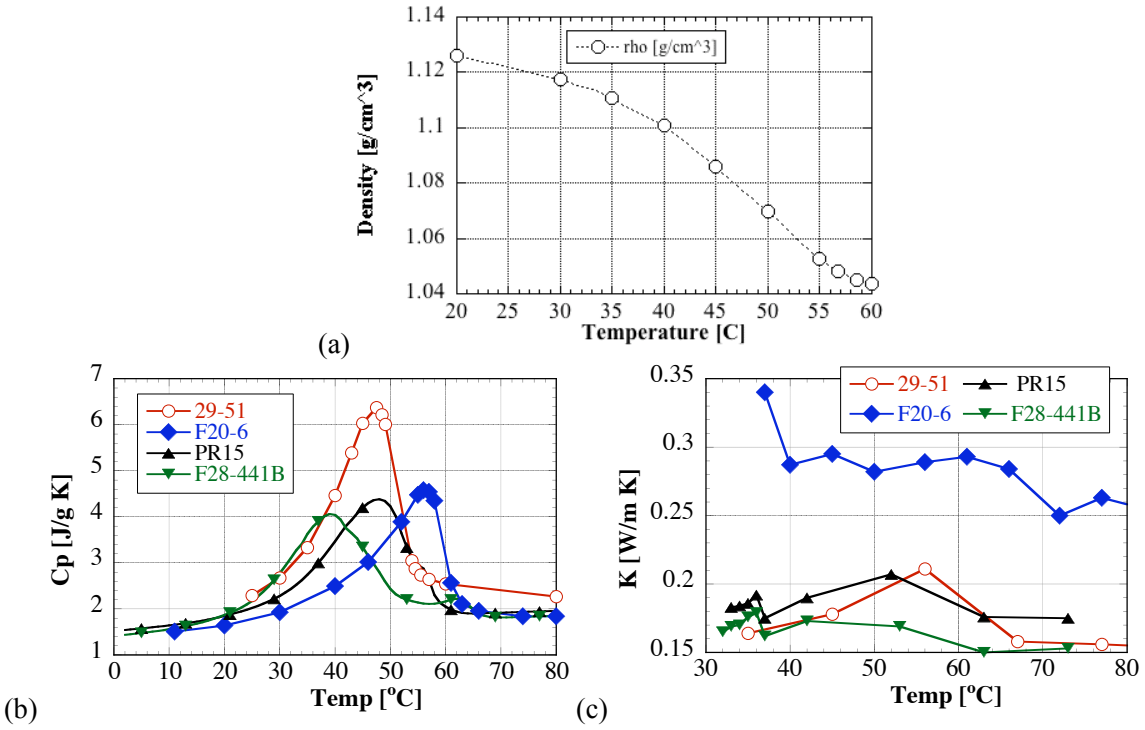

Figure 4.18. Density for Cerita™ F20-6 wax (a), specific heat (a) and thermal conductivity (b) for one unfilled wax, Cerita™ 29-51 wax, and three filled waxes.

4.3.2 Measurement techniques for thermomechanical properties of waxes

One of the main difficulties in using computer models for the prediction of wax dimensions is the lack of material properties of the wax. In particular, data on thermomechanical properties of waxes are scarce or nonexistent. The measurement of viscoelastic properties of waxes is not a trivial task since the investment casting waxes are complex blend of polymers that exhibit a wide range of behaviors (Sabau, 2004). Waxes used in the investment casting industry are a blend of semi-crystalline polymers, additives and fillers. For waxes tested, the glassy region occurs at temperatures below 20 ^{o}C. As temperature increases, waxes soften gradually. It was only recently that Sabau and Viswanathan (2000 and 2001) reported on a successful measurement of the thermomechanical properties of Cerita™ 29-51, a commercial, semi-crystalline, unfilled wax. Although Cerita™ 29-51

wax is a semicrystalline material, Sabau and Viswanathan (2000 and 2001) showed that in a paste state, the wax is a thermo-rheologically simple material that obeys the time-temperature superposition principle.

As waxes are viscoelastic materials, their thermomechanical properties can be determined using measurements techniques that were developed for polymers, such as dynamical mechanical analysis (DMA) measurements (Menard, 1999). In (DMA) tests, an oscillatory strain is applied to the material and the resulting stress is separated into elastic and viscous components. There are several ASTM standards for conducting DMA measurements and other industries have their own standards (Table 4.15).

Table 4.15 ASTM Standard for the DMA.

ASTM Standard	*Test description*
D4440	Measurement of Polymer Melts
D5023	DMA in Three Point Bending
D5024	DMA in Compression
D5026	DMA in Tension
D5279	DMA of Plastics in Tension
D5418	DMA in Dual Cantilever
D6648-01	BBR*: Flexural Creep Stiffness of Asphalt Binder (Standard)
D4 P 245	BBR: Flexural Creep Stiffness of Asphalt Binder (Test)

*BBR Flexural Creep Stiffness of Asphalt Binder

The wax material was tested using various fixtures and different instruments with higher sensitivity until appropriate test instruments, procedures, and fixtures were identified (Table 4.16). In Table 4.16, few other measurement techniques used in the investment casting community were also included. Based on our experience in measuring the viscoelastic properties of waxes and review of polymer testing, tests and fixtures, which we recommend for wax testing, are highlighted in Table 4.17. The tests and fixtures depend on material consistency.

It was observed that waxes exhibit a transition from a soft paste to that of a viscous liquid with less elasticity at a certain temperature, which is less than the melting point. For the sake of simplicity we refer to that temperature as the softening point temperature, T_{SP}. T_{SP} is given by the temperature at which the thermal expansion curve and DSC curve attain their peaks. T_{SP} can be associated with either an α transition for the crystalline component of the wax or a transition in the amorphous component of the wax. The former is due to the slippage of the crystallites past each other while the latter is related to the movement of coordinated segments reducing the viscosity (Menard, 1999).

Table 4.16. Tests used for determining wax properties

Property	*Tests/Sample shape*	*ASTM Standard*	*Test instruments*
Density and thermal expansion	Thermomechanical analysis (TMA)	E831	Dupont TMA
Specific heat (latent heat for phase changes)	Differential scanning calorimetry (DSC)	E1269 (ISO 11357)	Netzsch DSC 404C
Thermal conductivity	Transient line-source technique	D 5930-97	
Shear modulus (liquid)[1, 3]	Shear oscillatory: melt rheology/parallel plate	D4440-01	RFSII rheometer (RS)[2]
Shear modulus (liquid)	melt rheology/cone, concentric cylinder, capillary	D4440-95A, D3835-02	Rotational viscosimeter and capillary rheometer
Shear modulus (paste)[3, 4]	Torsion oscillatory/ rectangular geometry	D5279 (ISO 6721)	Advanced Rheometric Expansion System (ARES) (RS)[2]
Shear modulus (paste)[3, 4]	Shear oscillatory/disk	D5279 (ISO 6721)	DMTA IV (RS)[2]

[1]liquid, temperature above the ring and ball softening point
[2]RS indicates Rheometrics Scientific.
[3]For the wax tested, at temperatures of 60, 65, and 70^{o}C, reproducible data could not be obtained using either the Rheometrics Scientific ARES or melt rheometers.
[4]Bending beam rheometer may provide better data than the ARES system in the solid state.

Table 4.17. Tests and fixtures recommended for investment casting waxes.

Stiffness/ material form	**Test**	**Instrument (ASTM)**	**Fixture**	**Temperature range [^{o}C]**
Hard/solid	Flexural (3-pt. Bending)	BBR (D6648) 3-pt. (D5023)	Rectangular bar	RT< T < 40 (BBR) RT< T < T_{SP}-5 (3-pt)
Hard/hard paste or Soft/paste	Torsion oscillatory	DMA (D5279)	Rectangular bar	RT< T < T_{SP}-5
Soft and Gooey/ Paste	Shear oscillatory	DMA (D4440)	Disk	T_{SP}-10< T < T_{SP}
Liquid	Shear oscillatory	Melt rheometer (D4440)	Disk	T_{SP}+5< T <T_{SP}+20

4.3.3 Viscoelastic property data of filled waxes

Experimental data on thermomechanical properties were first obtained for Cerita F20-6, a commercial, filled wax. The DMA testing for Cerita^{TM} F20-6 wax using the bending-beam-rheometer (Sabau, 2004) was incomplete since the BBR method/fixture, which was originally designed for testing asphalt binders, could only be used for temperatures less than 40 ^{o}C. The shear modulus was determined from DMA measurements using the torsion bar fixture at Abatech, Inc. The wax was melted, stirred to suspend filler as much as possible and poured into a mold to form torsion rectangular sample approximately 50x12x3 mm. This sample was allowed to cool and when solidified the beam was mounted in a Rheometrics ARES DSR and tested. The test was a temperature frequency sweep from 20°C to 50°C in 10°C increments covering the frequency range of 0.05 to 100 radians/sec using 10 test points per decade. The targeted strain level was 0.15%. A strain sweep had been conducted at 35°C (the mid point of the temperature range) and we found that at 0.15% strain we were at 94.8% of the initial complex modulus G* value measured at 0.01% strain. The two sets of

data are measured from DMA are shown in Figure 4.19. This data is not ready for the direct use in computer simulation software and it must be post-processed to obtain data in a simpler format as shown in Appendix A. The post-processing steps are described in the remainder of this section.

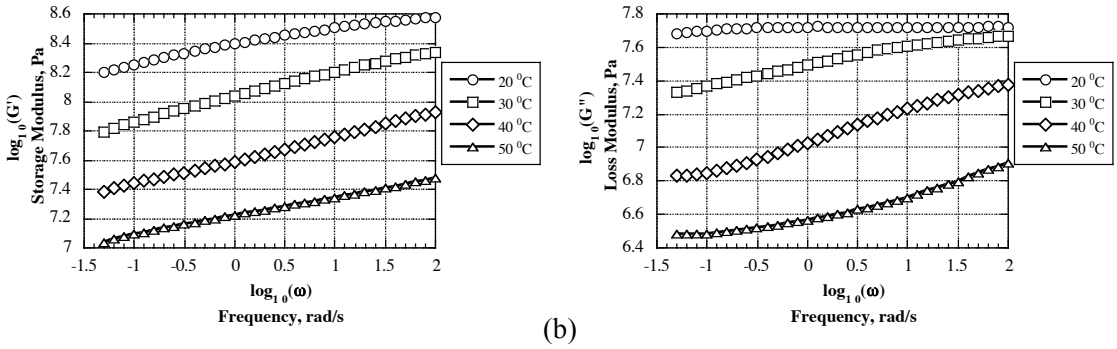

(a) (b)

Figure 4.19. DMA experimental results for the (a) storage shear modulus, and (b) the loss shear modulus as a function frequency (Cerita™ F20-6 wax, torsion geometry at Abatech, Inc.).

The three filled waxes were tested at the High Temperature Materials Laboratory (HTML) at ORNL using a DMA Q800 machine (TA Instruments, Inc.). It is worth noting that a different fixture and rheometer was used at ORNL than at Abatech, Inc., where the original measurements for Cerita™ F20-6 wax were performed. Thus, to insure testing consistency and compatibility between the measurements at ORNL and Abatech, Inc., F20-6 wax was tested first. The HTML wax samples were molded into a die tool that was designed and manufactured at industrial partners. The wax sample tested at ORNL using DMA Q800 had the following dimensions 60 x 10 x 4 mm. DMA measurements were performed using a 3-point bend fixture from 0 to 55 ^{o}C at 5 ^{o}C temperature increments. The slender beam of wax was simply supported and loaded with a constant force at mid span. The deflection was monitored with time and used for calculation of stiffness as a function of time. The raw data from the DMA measurements are shown in Appendix B for all the three filled waxes considered. The data on storage and loss modulus, which are shown in tables in the Appendix, were calculated for the Youngs modulus, and not for the shear modulus. The shear modulus, G, can be obtained from Youngs modulus, E, as:

$$G = E / (2 * (1+\nu)) \qquad (4.7)$$

where ν is the Poisson ratio. In Figure 4.20, the shear modulus data is shown for the CeritaTM F20-6 wax. However, the data at 55 ^{o}C was discarded as the sample yielded during the run at 55 ^{o}C.

After shifting the data horizontally, continuous curves were obtained over a very large frequency scale for both of the loss and storage moduli (Figure 4.21a and 4.21b). For Cerita F20-6, the shape of the master curve obtained at torsion and 3-point bending are in excellent agreement. The data on bending DMA shows larger values than those obtained on torsion DMA. This effect needs to be further understood. The same extent of horizontal shifting was applied to both the storage modulus, *G'*, and loss modulus, *G"* (Rowe and Sharrock, 2000). The fact that it was possible to obtain continuous master curves for both moduli over very large frequency ranges by the use of the same shift factors proves that the time-temperature superposition principle can be applied to the wax considered. The shift factors, defined as shown in Appendix B, were obtained for both sets of data (Figure 4.22). For Cerita F20-6, the shift factors obtained at torsion and 3-point bending are in excellent agreement, validating the use of 3-point bending testing for filled waxes.

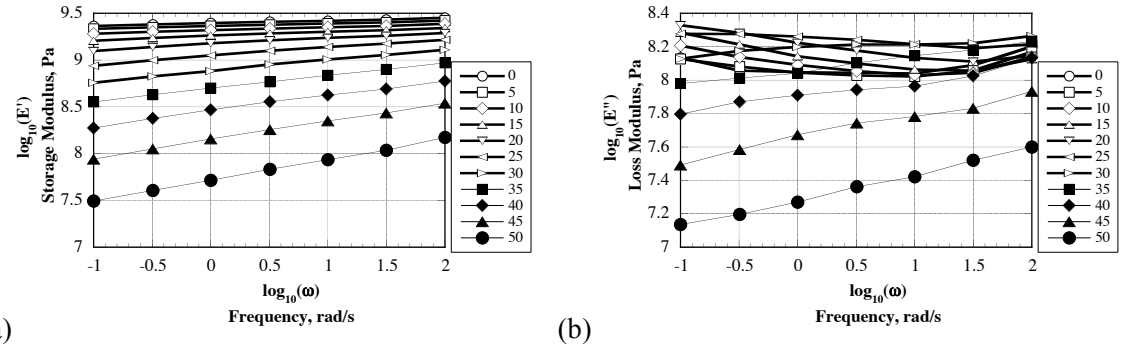

(a) (b)

Figure 4.20: DMA experimental results for the (a) Youngs loss modulus, and (b) Youngs storage modulus as a function of frequency (3-point bending).

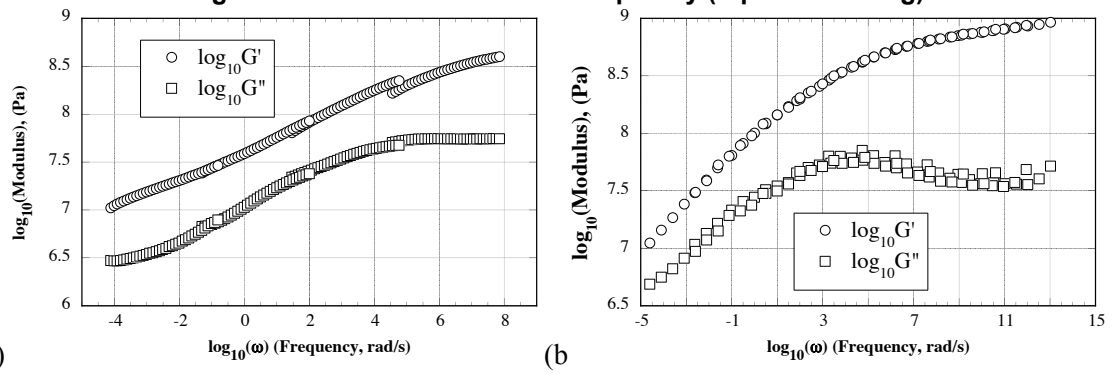

(a) (b

Figure 4.21. Master curves for the storage (G') and loss moduli (G") at the reference temperature of 40°C from experimental data on (a) torsion and (b) 3-point bending (Cerita™ F20-6 wax).

The next step was to perform a nonlinear regression from the master curves for the storage modulus, *G'*, and loss modulus, G", in order to obtain Prony series terms (Appendix A), which are the material parameters that can be used directly in computer simulation software (Sabau and Viswanathan, 2000). This analysis was performed for the DMA on torsion at Abatech, Inc. and the data for the Prony series is shown in Appendix B. The DMA data for the Cerita F20-844B and Remet PR-15 waxes, which is shown in Appendix C, need to be post-processed in the same manner as that for Cerita F20-6 in order to obtain data for computer simulation software**.**

For the first time in the investment casting industry, the thermo-mechanical properties of unfilled and filled waxes were measured. Recommendations were made to Investment Casting Institute on measurement techniques for waxes. Recommendations for mechanical testing of waxes were made based on testing one unfilled wax and one filled wax. The recommendations made could be used to establish new testing guidelines for waxes in the investment casting industry.

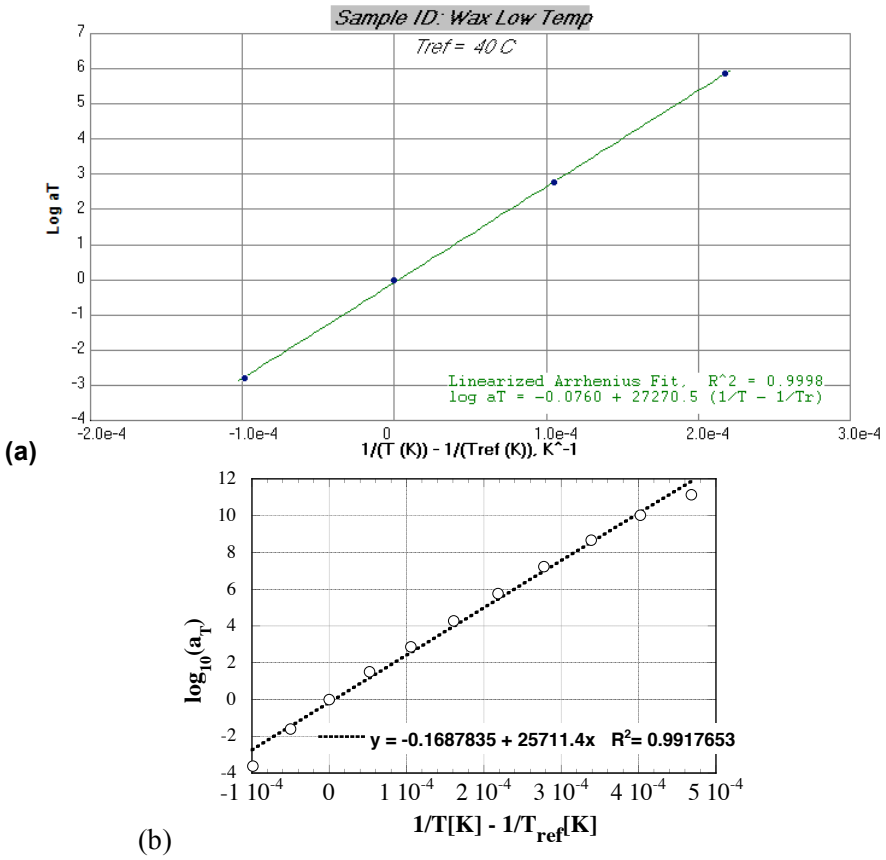

Figure 4.22: Linearized Arrhenius shift factor experimental data at T_{ref} = 40°C on (a) torsion and (b) 3-point bending (Cerita™ F20-6 wax).

It was found that dynamical mechanical analysis (DMA) can be used to analyze both elastic and viscous behavior of filled waxes. As the ASTM standards for DMA were developed for other applications and industries than those in investment casting, the study for the applicability of ASTM standards to investment casting waxes was initiated and partially completed. Results for DMA performed on torsion were obtained for one filled wax, Cerita F20-6. Results for DMA performed on 3-point bending were obtained for three filled waxes. For Cerita F20-6, the shape of the master curve and the shift factors obtained at torsion and 3-point bending are in excellent agreement, validating the use of 3-point bending testing for filled waxes.

5. Accomplishments

For convenience, a web site containing pertinent papers, reports and other information on this project has been established at http://www.ms.ornl.gov/mpg/sabau.htm.

5.1 Shell Mold

The data on properties of alumino-silicates materials used for shell molds are reviewed and material property data, which were not available from material suppliers, was obtained.

5.2 Alloy Shrinkage Factors

This study is the first attempt to predict shrinkage factors for the investment casting of stainless steels. The experimental data for 17-4PH stainless steel, did not cover the entire temperature range necessary for process simulation. Some property data had to be estimated using CompuTherm methodologies and recommendations from ProCAST. A comparison between the predicted material property data and measured property data was made. It was found that most material properties were accurately predicted only over several temperature ranges. No experimental data for plastic modulus were found. Thus, several assumptions were made and ProCAST recommendations were followed in order to obtain a complete set of mechanical property data at high temperatures. Thermal expansion measurements for the 17-4PH alloy were conducted during heating and cooling. As a function of temperature, the thermal expansion for both the alloy and shell mold materials showed different evolution on heating and cooling.

Numerical simulations were conducted to predict the alloy tooling allowances based on a combined analysis of heat transfer and deformation phenomena for 17-4PH stainless steel parts. Although the numerical results showed that the shrinkage evolution in time was quite different for the α_{heat} and α_{cool} cases, there was only a small difference in the final shrinkage factors predicted for these cases. The shrinkage factors were over-predicted for both the unrestrained dimensions and restrained dimensions. However, the effect of reduced shrinkage for restrained dimensions was adequately reproduced. With the exception of the L2_5 results for the no-hole part, the predicted shrinkage values are close enough to the measured values to allow a quantitative prediction of the shrinkage factors. The over-prediction of shrinkage values are likely due to assumptions used in the mechanical properties, especially at high temperatures, for which no experimental data were available.
In this section, the first attempt to determine shrinkage factors for the investment casting of stainless steels is presented. For all the properties of 17-4PH stainless steel, the experimental data available in the literature did not cover the entire temperature range necessary for process simulation. Thus, some material properties were evaluated using ProCAST, based on CompuTherm database.

5.3 Wax Properties

For the first time in the investment casting industry, the thermo-mechanical properties of unfilled and filled waxes were measured. Recommendations were made to Investment Casting Institute on measurement techniques for waxes. Recommendations for mechanical testing of waxes were made based on testing one unfilled wax and one filled wax. The recommendations made could be used to establish new testing guidelines for waxes in the investment casting industry.

In this report, material property data that is needed to determine dimensional changes associated with the wax system are provided. The following waxes were chosen by participating companies for testing: Cerita F20-6, Cerita F20-844B, and Remet PR-15. It was found that dynamical mechanical analysis (DMA) can be used to analyze both elastic and viscous behavior of filled waxes. As the ASTM standards for DMA were developed for other applications and industries than those in investment casting, the study for the applicability of ASTM standards to investment casting waxes was initiated and partially completed. Results for DMA performed on torsion were obtained for one filled wax, Cerita F20-6. Results for DMA performed on 3-point bending were obtained for three filled waxes. For Cerita F20-6, the shape of the master curve and the shift factors obtained at torsion and 3-point bending are in excellent agreement, validating the use of 3-point bending testing for filled waxes.

5.4 Technology Transfer

The techniques developed and material property data obtain in this project were documented in several publications and conference presentations. Detailed reports on alloy and shell mold materials were also issued to the participating companies. Through the ORNL work conducted in this project, the areas of material property measurement and modeling of material behavior has matured, allowing the software vendors to develop appropriate modules in their codes, the next steps in technology transfer. Over the course of the project, ORNL assisted ProCAST with advice, information, material property data, mesh files, ProCAST setup files, allowing immediate dissemination of the information to industry.

Recommendations were made to Investment Casting Institute on measurement techniques for waxes. Recommendations for mechanical testing of waxes were made based on testing one unfilled wax and one filled wax, both used by the industry. The recommendations made could be used to establish new testing guidelines for waxes in the investment casting industry.

5.5 Publications and Patents Resulting from Project

This project resulted in the following conference papers and archival journal articles reflecting results throughout the project:

Sabau, A.S., 2004, “Tests For Determining Viscoelastic Properties Of Investment Casting Waxes,” Paper No. 1, 48th Annual Technical Meeting, Investment Casting Institute.

Sabau, A.S., 2005, "Numerical simulation of the investment casting process," Transactions of American Foundry Society, 2005, paper 05-160, pp. 407-417.

Sabau, A.S. 2006, "Alloy Shrinkage Factors For The Investment Casting Process,” Metallurgical and Materials Transactions B, Vol. 37B, pp. 131-140.

Sabau, A.S. 2006, Prediction of Alloy Shrinkage Factors for the Investment Casting Process, 110th Metalcasting Congress, April 18-21 2006, Columbus, OH, paper 06-004.

Sabau, A.S. 2007, Shrinkage Prediction for the Investment Casting of Stainless Steels, 111th Metalcasting Congress, May 15-18 2007, Houston, TX, paper 07-042.

Sabau, A.S. and Porter, W.D., 2007, Alloy Shrinkage Factors for the Investment Casting of 17-4PH stainless Steel Parts, In print “Metallurgical and Materials Transactions B.” 2008.

6. Conclusions

In this study, the alloy shrinkage factors were obtained using numerical simulations for the first time for the investment casting of 17-4PH stainless steel parts, a high melting point alloy. There is a high probability that the experimental data available in the literature for material properties did not cover the entire temperature range necessary for process simulation. Thus, assumptions must be made in order to obtain material property data, especial mechanical properties at high temperature. The alloy dimensions were obtained from numerical simulation results of solidification, heat transfer, and deformation phenomena. As compared with experimental results, the numerical simulation results for the shrinkage factors were over-predicted.

For the first time in the investment casting industry, the thermo-mechanical properties of unfilled and filled waxes were measured. Recommendations were made to Investment Casting Institute on measurement techniques for waxes. Recommendations for mechanical testing of waxes were made based on testing one unfilled wax and one filled wax. The recommendations made could be used to establish new testing guidelines for waxes in the investment casting industry.

It was found that dynamical mechanical analysis (DMA) can be used with confidence to analyze both elastic and viscous behavior of filled waxes. As the ASTM standards for DMA were developed for other applications and industries than those in investment casting, the study for the applicability of ASTM standards to investment casting waxes was initiated and partially completed. For Cerita F20-6, the shape of the master curve and the shift factors obtained at torsion and 3-point bending are in excellent agreement, validating the use of 3-point bending testing for filled waxes. The data on bending DMA shows larger values than those obtained on torsion DMA. This effect needs to be further understood.

These findings are very important for future investigations and for the enhancement of commercial investing casting software. Pending availability of material property data, the computer simulation software is mature enough to *quantitatively* predict shrinkage factors for high melting point alloys with an accuracy less than that for light cast alloys.

7. Recommendations

Prediction of shrinkage factors with high accuracy is possible in the investment casting industry, pending that material properties are measured and appropriate material models are available in commercial casting software. In order to obtain data for a specific foundry, combined experimental and computational programs must be conducted. The experimental program should concentrate on measuring material properties. The experimental program could be relatively small, since it could be carried only once for each material. Based on the results presented in previous sections, the following recommendations were made for the use of numerical simulation in the investment casting process.

7.1 Shell

Additional work must be performed to account for creep properties during investment casting of heavy sections. Recommendations for the shell mold presented in the progress report for phase II need to be followed (Sabau, 2005).

7.2 Alloy

Several assumptions need to be made in order to obtain a complete set of mechanical property data at high temperatures. The quality of the estimated data based on assumptions need to be assessed by comparison with experimental data. Due to phase transformations, the thermal expansion of the alloy is different on cooling than on heating. Thermal expansion data for the alloy must be obtained on cooling, not on heating, as is usually reported in the literature.

7.3 Wax

The users need help in dealing with the post-processing of the DMA data. Commercial software vendors, such as ProCAST to bridge the gap between the raw data provided by measurements and the data needed in viscoelastic models in a simpler format, such as the shift factor and Prony series. The computer implementation of this post-processing would have the benefit of reducing the cost for testing the wax material and enabling more resources towards the simulations. Another possibility would be to take as input the creep test data for a viscoelastic material, without asking the user for Prony series.

7.4 Technology Transfer

Additional work is needed to enhance the wax model. The viscoelastic module implemented in ProCAST needs to be validated. Mechanical properties for the alloy, especially at high temperature need to be measured.

Echoing the foundry industry needs, the project steering committee members informed the wax suppliers of the increasing demand for wax properties. Foundries can now effectively use the wax property data as the new wax module was recently added to the software suite for the investment casting by ProCAST. The commercialization of wax module will provide an incentive for the wax suppliers to provide the data on mechanical properties of waxes, whose use in foundries will lead to significant advances in the investment casting industry.

8. References

Abdella, K., International Journal of Non-Linear Mechanics, Vol. 41, 2006, pp. 456-463

Achari, S. and L.N. Satapathy, Mullite-Based Refractories for Molten-Metal Applications, American Ceramic Society Bulletin, Vol. 82, pp. 2, 2003.

AK Steel, Product Data Bulletin, http://www.aksteel.com/markets_products/stainless_precipitation.asp

ASM alloy Center: Materials Property Data, http://products.asminternational.org/matdb/index.jsp

Atlas of Formability, Concurrent Technologies Corporation, 1996, http://www.nmc.ctc.com/ekb/ekb_atlas.cfm

Bellet, M.; Decultieux, F.; Menai, M.; Bay, F.; Levaillant, C.; Chenot, J. L.; Schmidt, P.; and Svensson, I. L. 1996, "Thermomechanics of the Cooling Stage in Casting Processes: Three-Dimensional Finite Element Analysis and Experimental Validation," *Metallurgical and Materials Transactions,* Vol. 29B, pp. 81–99.

Browne, D.J., and Sayers, K., 1995, "Experimental Measurement of Investment Shell Properties and Use of the Data in Casting Simulation Software," Proc. 7-th Conference Model. Casting Welding Adv. Solid. Process.

Chen, S. L.; F. Zhang, S. Daniel, F. Y. Xie, X. Y. Yan, Y. A. Chang, R. Schmid-Fetzer, W. A. Oates, "Calculating phase diagrams using PANDAT and PanEngine," JOM, 2003, vol. 55, pp. 48-51.

Chen, J. and Young, B., 2006, Vol. 28, pp. 229-239.

Drezet, J.-M., and Rappaz, M. 1996. "Modeling of Ingot Distortion during Direct Chill Casting of Aluminum Alloys," *Metallurgical and Materials Transactions,* Vol. 27A, pp. 3214–3225.

Fachinotti, V. D. & Cardona A., J. of Materials Processing Technology, Vol. **135**, pp. 30-43, 2003

Fieldhouse, I. B. and Lang J. I., Measurement of Thermal Properties, Wright Air Development Division, Report 1-119, 1961.

Frankel, J.I. Porter, W.D., and Sabau, A., Journal of Thermal Analysis and Calorimetry, 2005, Vol. 82, pp. 171-177.

Fukuhara, M. and A. Sanpei, Japanese Journal of Applied Physics, Vol. 33, pp. 2890-2893 (1994).

Goodson, C.C., Simulation of Microwave Heating of Mullite Rods, Master's Thesis, Virginia Polytechnic Institute and State University, 1997

Guo J, Samonds MT, Journal of phase equilibria and diffusion, Vol. 28, pp. 58-63, 2007.

Hammond VH, Elzey DM, Elevated temperature mechanical properties of partially sintered alumina, Composites Science and Technology, vol. 64, pp. 1551-1563, 2004.

Irvine, K.J. et al, Controlled-transformation stainless steels, in The Metallurgical Evolution of Stainless Steels, ed. F.B Pikering, American Society for Metals, Metals Park, Ohio, 1979, pp. 121-141.

Jones S.; Jolly M.R.; Lewis K. Development of techniques for predicting ceramic shell properties for investment casting, British Ceramic Transactions, Volume 101, pp. 106-113.

Kajitani, T., Drezet, J.-M. and M. Rappaz, *Met. Mater. Trans.*, Nr. 32A, pp. 1479-88, 2001.

Kozlowski, P. F., J. A. Azzi, B. G. Thomas and H. Wang, Metallurgical Transactions A, Vol. 23A, 1992, pp. 903-918.

Menard, K.P., 1999, "Dynamic Mechanical Analysis: A Practical Introduction to Techniques and Applications," CRC Press, Boca Raton, Florida.

Metallic Materials Properties Development and Standardization (MMPDS). U.S. Department of Transportation, 2003.

Munro RG, Analytical representations of elastic moduli data with simultaneous dependence on temperature and porosity, Journal of Research of the National Institute of Standards and Technology, Vol. 109, pp. 497-503, 2004.

Munro RG, Effective medium theory of the porosity dependence of bulk moduli, Journal of the American Ceramic Society, vol. 84, pp. 1190-1192, 2001.

Munro RG, Evaluated Material Properties for a Sintered alpha-Al_2O_3, Journal of the American Ceramic Society, Vol. 80, pp. 1919-1928,1997.

Perzyna, P.: *Quarterly Applied Math*., 1963, vol. 20, pp. 321-332.

Porter, W.D. and Maziasz, P.J., Scripta Metallurgica et Materialia, 1993, Vol. 29, pp. 1043-1048.

Pierer, R., Bernhard, C. and C. Chimani, Transactions on Modelling and Simulation, Vol 41, 20-22, Malta (2005), pp. 757-768.

O'Mahoney D., Browne D.J., "Use of Experiment and an Inverse Method to Study Interface Heat Transfer During Solidification in the Investment Casting Process", Exper. Ther. Fluid Sci., 22(3-4), 2000, pp. 1-12.

Rack, H.J., 1981, "Physical and Mechanical Properties of Cast 17-4 PH Stainless Steel," 1981, Sandia Report, SAND-80-2302, TTC-0161, Issued Febr. 1981.

Rowe, G. M., and Sharrock, M. J. 2000. "Development of Standard Techniques for the Calculation of Master Curves for Linear-Visco Elastic Materials," First International Symposium on Binder Rheology and Pavement Performance, University of Calgary, Alberta, Canada, August 14–15.

Russell, L. M., L. F. Johnson, D.P.H. Hasselman, and R. Ruth, 'Thermal Conductivity/Diffusivity of Silicon Carbide Whisker Reinforced Mullite', J. Am. Soc. Vol. 70:C-226-229, 1987.

Sabau, A.S., Metallurgical and Materials Transactions, 2006, Vol. 37B, pp. 131-140.

Sabau, A.S. and Viswanathan, S., Thermophysical Properties of Zircon and Fused Silica-based Shells used in the Investment Casting Process, Transactions of American Foundry Society, 2004, Vol. 112, paper 04-081

Sahai V. and R.A. Overfelt: AFS Trans., 1995, vol. 103, pp. 627–32.

Sabau, A. S. 2005. "Numerical Simulation of the Investment Casting Process," *Transactions of American Foundry Society,* paper 05-160.

Sabau, A. S., and Viswanathan, S. 2000. "Material Properties for Predicting Wax Pattern Dimensions in Investment Casting," Paper No. 4, 48th Annual Technical Meeting, Investment Casting Institute, Dallas, TX, Oct. 15–18.

Sabau, A. S., and Viswanathan, S. 2001. "Determining Wax Pattern Dimensions in Investment Casting Using Viscoelastic Models," Paper No. 3, 49th Annual Technical Meeting, Investment Casting Institute, Orlando, FL, Oct. 7–10.

Sabau, A. S., and Viswanathan, S. 2003. "Material Properties for Predicting Wax Pattern Dimensions in Investment Casting," *Materials Science & Engineering A,* Vol. 362A, pp. 125–134.

Sabau, A. S., and Viswanathan, S. 2001. "Critical Material Properties for Predicting Pattern Tooling Dimensions in Investment Casting," *Transactions of American Foundry Society,* Paper No. 01-017, pp. 1–18.

Sabau, A. S., and Viswanathan, S. 2001. "Numerical Simulation of Wax Pattern Dimensions in Investment Casting," Proceedings of Computational Modeling of Materials, Minerals, and Metals Processing, 2001 Annual Fall TMS Meeting, San Diego, CA, Sept. 23–26, pp. 431–440.

Sabau, A. S., and Viswanathan, S. 2001. "Determining Wax Pattern Dimensions in Investment Casting Using Viscoelastic Models," Investment Casting Institute 49th Annual Meeting, Orlando, FL, October 7–10, 2001, paper no. 3.

Sandmeyer Steel Company, 2005, Property data sheet, http://www.stainlessplate.com/images/17-4PH-Spec-Sheet.pdf

Schwerdtfeger, K.; M. Sato, and K-H. Tacke: *Metallurgical and Materials Transactions*, 1998, vol. 29B, pp. 1057-1068.

Snow, J. D., in *Proceedings of 43rd Annual Meeting of the Investment Casting Institute*, Dallas, TX, 1995, Oct. 29-Nov. 1, Paper no. 18.

Snow, J. D., 2004, personal communication.

Straton, R. R., et al. *Ceramics Testing Guidebook,* Investment Casting Institute.

Touloukian, Y.S., *Thermal Radiative Properties*, Vol. 8, New York-Washington, p.142, 1972.

Touloukian Y. S. et al., 1979, Thermophysical Properties of Matter, (now Thermophysical Properties of Matter Database, https://cindasdata.com)

Wereszczak, A. A., K. Breder, M.K. Ferber, T.P. Kirkland, A. Payzant, C. Rawn, E. Krug, C. L. LaRocco, R.A. Pietras, and M. Karakus, "Dimensional Changes and Creep of Silica Core Ceramics Used in Investment Casting of Superalloys," Journal of Mat. Science, 37 4235-45 (2002).

Waite, D. M., and Samonds, M. T. 1990. "Finite Element Solidification Analysis of Investment Castings," 38th Annual Technical Meeting, Investment Casting Institute.

Weddington, V. L.; Reddy, G. P.; and Mobley, C. E. 1990. *Dimensional Control in the Investment Casting Process,* Report EMTEC/CT/TR-90-14, Edison Materials Technology Center, Dayton, OH.

Wu JH, Lin CK, Journal of materials science, 2003, vol. 38, pp. 965-971.

Appendix A. Thermo-Mechanical Models of Alloys

The analysis performed for the Atlas of Formability data is described below. According to the information from the Atlas of Formability, the plastic flow behavior of 17-4 PH stainless steel was studied by conducting compression tests at various temperatures (950- 1250 ^{o}C) and strain rates of 0.001:20 1/sec. The testing procedures involved isothermal compression tests on a servo-hydraulic MTS machine of cylindrical specimens with a diameter of 12.7 mm and a height of 15.9 mm. Load and stroke data were acquired during the tests and subsequently converted to true stress-true strain curves. The stress-strain curves available from the Atlas of Formability were used to estimate the yield stress at temperatures of 950 to 1250 ^{o}C. Typical true-stress true-strain data are shown in Figure A.1 at temperatures of 950 and 1250 ^{o}C for all the strain rates available. Data available at the strain rate of 0.001 1/sec shown in Figure A.2 was used to estimate the yield strength.

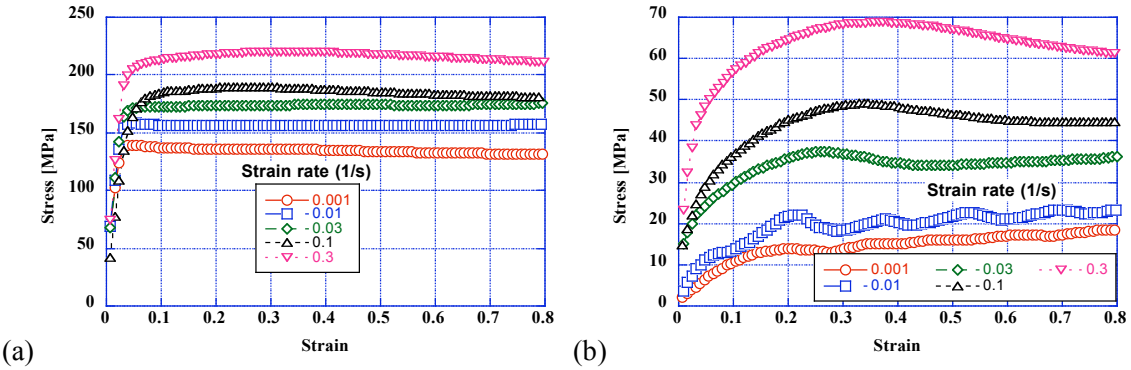

Figure A.1. True-strain true-stress data at temperatures of (a) 950 and (b) 1250 ^{o}C (Atlas of Formability).

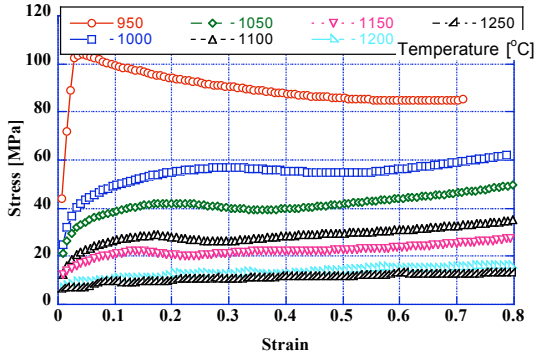

Figure A.2. True-strain true-stress data at a strain rate of 0.001 s^{-1} as a function of temperature used to estimate the yield stress (Atlas of Formability).

Appendix A References

Atlas of Formability, Concurrent Technologies Corporation, 1996, http://www.nmc.ctc.com/ekb/ekb_atlas.cfm

Appendix B. Constitutive Equations for Modeling Wax Deformation

The principle of time-temperature superposition is based on the observation that time and temperature have an equivalent influence on the viscoelastic properties; an increase in temperature corresponds to an extension of the time scale of the experiment. The frequency domain in the master curve must be large enough to cover the relevant domain for our process. As we can see from these relationships, if the shear modulus must be obtained over a time domain $\left[t_1 : t_2\right]$, the required frequency test domain is $\left[0.1/t_2 : 10/t_1\right]$. The time domain over which shear modulus is needed depends on size of the part and thermal diffusivity of waxes (Sabau, 2004) was estimated for small patterns of thickness less than one inch to be approximately [0:24hours], or [$0.01:10^5$] seconds. This would correspond to a frequency domain of [10^{-6}: 10^3] rad/seconds. The modulus for thermo-rheologically simple materials is given by

$$G(t-s,T) = G\left(\xi(t) - \xi(s), T_0\right), \tag{B.1}$$

where the reduced time, $\xi(t)$, is given as a function of the shift factor, a_T, as

$$\xi(t) = \int_0^t \frac{1}{a_T\left(T(\phi)\right)} d\phi \,. \tag{B.2}$$

For a generalized Maxwell-material, the shear relaxation modulus as a function of time, t, is given as

$$G(t) = g_0 + \sum_{i=1}^{N} g_i \exp\left(-t/\lambda_i\right), \tag{B.3}$$

where λ_i is the relaxation time and g_i is the relaxation strength. These material constants were determined by a nonlinear regression of the master curve data, using the IRIS software (Baumgaertel and Winter 1989), and are shown in Table B.1 for DMA data obtained using the torsion fixture data.

Table B.1. Relaxation times, λ_i, and relaxation strengths, g_i, determined from experimental measurements by nonlinear regression analysis at the reference temperature of 40°C for Cerita F20-6 wax (torsion DMA).

No.	g_i (Pa)	λ_i (s)	No.	g_i (kPa)	λ_i (s)
1	3.14e+08	1.97E-09	10	1.95e+07	3.54E-02
2	6.29e+07	4.63E-08	11	1.45e+07	1.97E-01
3	5.69e+07	2.55E-07	12	1.08e+07	1.18E+00
4	5.66e+07	1.36E-06	13	7.75e+06	7.22E+00
5	5.36e+07	7.43E-06	14	5.78e+06	4.71E+01
6	4.77e+07	4.09E-05	15	4.52e+06	3.35E+02
7	4.02e+07	2.25E-04	16	3.97e+06	2.67E+03
8	3.22e+07	1.22E-03	17	1.00e+07	5.65E+04
9	2.57e+07	6.51E-03			

Appendix B References

Baumgaertel, M., and Winter, H. H. 1989. "Determination of Discrete Relaxation and Retardation Time Spectra from Dynamic Mechanical Data," *Rheol. Acta,* Vol. 28, p. 511.

Sabau, A.S., 2004, "Tests For Determining Viscoelastic Properties Of Investment Casting Waxes," Paper No. 1, 48th Annual Technical Meeting, Investment Casting Institute.

Appendix C. DMA data from measurements conducted at HTML/ORNL

The DMA measurements were performed using a 3-point bend fixture from 0 to 55 °C at 5 °C temperature increments. The raw data from the DMA measurements are shown in this Appendix for all the three filled waxes considered in Tables C1, C2, and C3. The data on storage and loss modulus shown in these tables were calculated the Youngs modulus, and not for the shear modulus. The storage and loss modulus were evaluated in Tables C1-3 using the following relationships:

Modulus = Stiffness * GF (C.1)

$$GF = \frac{0.25}{W}\left[\left(\frac{L_o}{H}\right)^3 + 0.75(1+\upsilon)\frac{L_o}{H}\right] \quad \text{(C.2)}$$

GF was the geometry factor, given above for the 3-point bending test. The distance between the clamps *Lo* was 50 mm. The thermal expansion of the wax was not considered when the storage and loss modulus were evaluated in the tables below, i.e., the sample width and thickness were 10 and 4 mm. The values shown in the three tables below can be changed to account for the thermal expansion of the wax by allowing for a temperature dependence of the width and thickness dimension in the geometry factor shown above. This thermal expansion conversion was performed for the result shown in the body of the report for Cerita F20-6 wax.

Table C1. DMA results for Cerita F20-6 wax.

Time	Temp.	Youngs Storage Modulus	Youngs Loss Modulus	Stress	Freq.	Drive Force	Amplitude	Strain	Displace-ment	Static Force	Position	Length	Force	Stiffness
(min)	(°C)	(MPa)	(MPa)	(MPa)	(Hz)	(N)	(µm)	(%)	(µm)	(N)	(mm)	(mm)	(N)	(N/m)
16.2907	-4.78E-03	2263.87	133.686	0.215952	0.1	0.463897	9.99926	0.00953904	42.0452	0.572541	3.1894	50.0418	0.472287	47232.1
44.7935	4.97162	2127.6	132.095	0.202969	0.1	0.436582	10	0.00953978	46.8486	0.579749	3.19421	50.0475	0.443893	44389.1
72.102	9.94321	1891.96	159.447	0.180668	0.1	0.390074	10.01	0.00954924	47.5955	0.514014	3.19493	50.0477	0.395121	39472.7
99.7457	14.9468	1603.97	191.309	0.153252	0.1	0.332911	10.0155	0.00955454	48.1825	0.429428	3.19548	50.048	0.335162	33464.3
127.821	19.9488	1248.99	213.035	0.119298	0.1	0.261883	10.0124	0.00955157	47.141	0.338631	3.1944	50.0472	0.260904	26058.1
155.694	24.9678	871.731	190.298	0.083218	0.1	0.184966	10.0069	0.00954629	40.0769	0.23875	3.18729	50.0404	0.181998	18187.3
183.873	29.9772	577.683	135.51	0.0552325	0.1	0.12356	10.0223	0.00956104	52.1502	0.156965	3.19933	50.0523	0.120793	12052.4
212.41	34.9795	363.911	97.1682	0.0346992	0.1	0.0784081	9.99512	0.00953509	96.9641	0.0986726	3.24412	50.097	0.0758872	7592.42
242.387	39.9842	193.283	64.4409	0.0184252	0.1	0.0425144	9.99266	0.00953274	155.963	0.053063	3.3031	50.1558	0.0402959	4032.55
272.204	44.9911	91.4388	32.5279	0.0087347	0.1	0.0203687	10.0134	0.0095525	267.271	0.0253699	3.4144	50.2671	0.0191028	1907.73
302.498	50.006	33.4324	14.6521	0.00321093	0.1	0.0077709	10.0676	0.00960424	570.732	0.0098413	3.71785	50.566	0.0070223	697.514

Time	Temp.	Youngs Storage Modulus	Youngs Loss Modulus	Stress	Freq.	Drive Force	Amplitude	Strain	Displace-ment	Static Force	Position	Length	Force	Stiffness
(min)	(°C)	(MPa)	(MPa)	(MPa)	(Hz)	(N)	(µm)	(%)	(µm)	(N)	(mm)	(mm)	(N)	(N/m)
21.1596	0.00251995	2359.28	111.699	0.224714	0.32	0.482021	9.98424	0.0095247	43.3743	0.584771	3.19074	50.043	0.491451	49222.7
49.6624	5.00984	2202.02	118.797	0.210086	0.32	0.451414	10.0009	0.00954059	46.8875	0.56921	3.19424	50.0468	0.459457	45941.6
76.9709	9.99664	1983.7	135.909	0.189352	0.32	0.408012	10.0059	0.00954541	48.1368	0.508853	3.19547	50.0479	0.414113	41386.7
104.615	14.9921	1716.02	162.614	0.163853	0.32	0.354663	10.0091	0.00954841	49.1702	0.432642	3.19647	50.0488	0.358347	35802.1
132.69	19.9878	1383.11	191.702	0.132156	0.32	0.288361	10.016	0.00955499	48.2022	0.344578	3.19546	50.0477	0.289026	28856.5
160.563	2.50E+01	1003.67	189.444	0.0959185	0.32	0.211703	10.0178	0.00955674	41.0965	0.246388	3.18832	50.0405	0.209774	20940.1
188.742	29.994	674.834	151.113	0.0644729	0.32	0.143743	10.0148	0.00955388	55.9152	0.164339	3.2031	50.0544	0.141002	14079.3
217.279	35	433.892	104.643	0.0414334	0.32	0.0929639	10.01	0.00954925	103.089	0.105064	3.25025	50.1006	0.0906148	9052.46
247.256	39.9964	245.202	76.4638	0.0234091	0.32	0.0536187	10.0075	0.00954688	165.314	0.0588645	3.31245	50.1618	0.0511958	5115.75
277.073	44.9925	117.842	40.3585	0.0112314	0.32	0.0260434	9.99072	0.00953089	283.237	0.02825	3.43036	50.2774	0.0245631	2458.59
308.203	49.9922	43.2758	16.8287	0.0041298	0.32	0.0097912	10.0034	0.00954297	617.509	0.0106193	3.76463	50.5991	0.00903186	902.881
22.5552	-0.002518	2438.94	109.368	0.23261	1	0.498468	9.99748	0.00953734	44.0292	0.604188	3.1914	50.0439	0.508718	50884.6
51.0395	5.02103	2275.24	109.39	0.217104	1	0.465973	10.0024	0.00954204	47.055	0.573846	3.19441	50.047	0.474806	47469.2
78.348	9.99254	2067.86	122.296	0.197307	1	0.424504	10.002	0.00954164	48.4633	0.517405	3.1958	50.0484	0.431511	43142.5
106.03	15.0027	1818.54	138.235	0.173455	1	0.374428	9.99831	0.00953813	50.0447	0.451137	3.19735	50.0498	0.379346	37941
134.106	19.9946	1509.97	167.14	0.143998	1	0.31269	9.9966	0.0095365	49.5829	0.36902	3.19685	50.0492	0.314923	31503.1
162.085	24.9977	1129.61	183.031	0.107732	1	0.236348	9.99723	0.0095371	46.8509	0.294645	3.19409	50.0444	0.23561	23567.5
190.263	30.0005	770.366	159.324	0.0734492	1	0.162956	9.99432	0.00953432	60.6873	0.203061	3.20789	50.0498	0.160633	16072.5
218.7	34.9976	512.847	111.915	0.0489444	1	0.109101	10.0041	0.00954365	107.935	0.12386	3.2551	50.1068	0.107041	10699.7
248.679	39.9956	302.571	83.5944	0.0288353	1	0.0652907	9.98989	0.0095301	172.467	0.0733642	3.31961	50.1709	0.0630628	6312.66
278.521	44.9986	150.666	49.4533	0.0143834	1	0.0331065	10.0071	0.00954651	293.949	0.0367217	3.44108	50.2918	0.0314565	3143.42
309.582	5.00E+01	55.5134	19.9544	0.0052836	1	0.0123155	9.9769	0.00951771	634.828	0.0133317	3.78195	50.6329	0.0115552	1158.2
23.7008	0.0052952	2511.89	108.539	0.239548	3.2	0.512118	9.99667	0.00953656	44.757	0.623076	3.19214	50.0445	0.523892	52406.7
52.0165	5.02702	2349.74	105.066	0.224114	3.2	0.479777	9.99801	0.00953784	47.4622	0.585491	3.19483	50.0473	0.490138	49023.5
79.3248	10.0101	2147.59	112.052	0.204842	3.2	0.439383	9.9984	0.00953822	49.2061	0.531954	3.19655	50.049	0.44799	44806.1
107.346	1.50E+01	1914.27	125.227	0.182591	3.2	0.392673	9.99861	0.00953841	51.5696	0.473153	3.19889	50.051	0.399326	39938.2
135.422	20.0009	1627.49	150.353	0.155259	3.2	0.335328	10.0001	0.00953979	52.3105	0.397042	3.19959	50.0514	0.339551	33954.9
163.402	25.0027	1265.62	175.158	0.120659	3.2	0.262639	9.99359	0.00953362	50.3158	0.310508	3.19756	50.0491	0.263882	26405.1
192.305	30	906.248	165.101	0.0864297	3.2	0.189816	9.99723	0.0095371	75.7964	0.234279	3.22301	50.0671	0.189022	18907.4
220.377	34.9921	597.234	129.326	0.0569661	3.2	0.126028	9.99851	0.00953832	119.195	0.145388	3.26637	50.1145	0.124585	12460.4
249.999	39.9991	369.234	90.3202	0.0352253	3.2	0.078289	10.0004	0.00954008	187.774	0.0893434	3.33493	50.1829	0.0770376	7703.49
279.848	44.997	190.049	58.0324	0.0181253	3.2	0.0406425	9.99727	0.00953714	315.203	0.0460352	3.46234	50.3082	0.03964	3965.08
310.558	49.997	72.9216	24.626	0.00695286	3.2	0.0153217	9.99471	0.00953469	664.954	0.0174093	3.81208	50.6555	0.0152059	1521.39

Time	Temp.	Youngs Storage Modulus	Youngs Loss Modulus	Stress	Freq.	Drive Force	Amplitude	Strain	Displace-ment	Static Force	Position	Length	Force	Stiffness
(min)	(°C)	(MPa)	(MPa)	(MPa)	(Hz)	(N)	(µm)	(%)	(µm)	(N)	(mm)	(mm)	(N)	(N/m)
24.0963	-0.00821	2580.25	107.574	0.246127	10	0.5175	9.99908	0.00953887	45.2224	0.64116	3.19261	50.0451	0.538279	53832.8
52.3937	5.02453	2418.69	103.472	0.23075	10	0.485312	10.0006	0.0095403	47.8454	0.600308	3.19522	50.0477	0.504651	50462.1
79.7405	10.0246	2222.21	106.167	0.21198	10	0.445975	9.9994	0.00953917	49.898	0.552461	3.19725	50.0497	0.463601	46362.9
107.762	15.0023	1996.51	115.138	0.190439	10	0.400754	9.99883	0.00953862	52.5503	0.494782	3.19988	50.0523	0.416491	41654
135.838	19.9998	1726.89	135.74	0.164688	10	0.346694	9.99677	0.00953665	53.8564	0.423202	3.20115	50.0534	0.360172	36028.8
163.819	25.0108	1389.63	164.988	0.132562	10	0.279319	9.99956	0.00953932	52.703	0.337951	3.19996	50.052	0.289912	28992.5
192.723	29.9976	1026.88	164.835	0.0979035	10	0.205915	9.99402	0.00953404	78.3869	0.250801	3.22561	50.0776	0.214115	21424.3
220.798	35.0063	698.759	142.542	0.0666582	10	0.138988	9.99976	0.00953951	124.434	0.168109	3.27162	50.1228	0.145782	14578.5
250.42	4.00E+01	435.575	94.8187	0.0415273	10	0.0837693	9.9939	0.00953392	195.529	0.105439	3.34269	50.1935	0.0908203	9087.57
280.276	44.9986	235.367	63.5149	0.0224737	10	0.0421804	10.009	0.00954834	326.351	0.0570544	3.47349	50.3235	0.0491499	4910.57
311.121	49.9986	92.3245	28.2548	0.00880329	10	0.0119845	9.9952	0.00953516	709.532	0.0263505	3.85666	50.7064	0.0192528	1926.2
24.7002	0.00564271	2655.14	120.592	0.253224	31.6	0.448645	9.99726	0.00953712	45.8959	0.659297	3.19329	50.0457	0.553802	55395.4
52.9122	5.03E+00	2490.42	112.421	0.237513	31.6	0.415762	9.9972	0.00953707	48.3801	0.616555	3.19576	50.0482	0.519441	51958.7
80.4308	10.0246	2294.53	109.49	0.218862	31.6	0.376681	9.99863	0.00953843	50.7755	0.571476	3.19813	50.0505	0.478651	47871.7
108.452	15.0134	2074.98	113.509	0.197921	31.6	0.332779	9.99867	0.00953847	53.8874	0.515164	3.20122	50.0535	0.432854	43291.1
136.529	20.0086	1820.04	129.126	0.173601	31.6	0.28187	9.99847	0.00953828	56.2255	0.447801	3.20353	50.0554	0.379665	37972.3
164.511	25.0052	1507.07	155.931	0.143723	31.6	0.219646	9.99668	0.00953657	56.7074	0.366445	3.20398	50.0554	0.314322	31442.6
193.42	29.9973	1147.42	167.914	0.109449	31.6	0.148346	9.99891	0.0095387	84.1225	0.277171	3.23136	50.082	0.239364	23939
221.88	34.9997	809.367	154.194	0.0771433	31.6	0.0817464	9.99117	0.00953132	143.542	0.209976	3.29075	50.1363	0.168712	16886.2
251.228	39.9963	505.594	109.071	0.0481992	31.6	0.0273735	9.99311	0.00953317	211.254	0.122502	3.35842	50.205	0.105412	10548.4
281.055	44.9989	285.981	71.1598	0.0272866	31.6	0.0377228	10.0017	0.00954139	351.724	0.0697814	3.49887	50.3433	0.0596757	5966.54
311.991	49.9952	116.266	35.4453	0.0110881	31.6	0.0696304	9.99697	0.00953685	744.408	0.0288975	3.89153	50.7304	0.0242496	2425.7
24.9907	0.00087751	2779.26	155.864	0.265284	100	0.346467	10.0056	0.00954513	46.9039	0.701048	3.19432	50.0466	0.580176	57984.8
53.2012	5.02361	2611.4	145.181	0.249156	100	0.37939	10.0014	0.00954111	49.5027	0.659935	3.1969	50.0491	0.544904	54482.6
80.7213	10.018	2411.94	136.207	0.230142	100	0.418975	10.0021	0.00954175	52.0464	0.612352	3.19942	50.0516	0.50332	50321.3
108.761	15.0125	2194.04	132.923	0.209345	100	0.462481	10.0018	0.0095415	55.7559	0.5614	3.20311	50.0551	0.457837	45775.2
136.838	20.0243	1945.65	139.783	0.185634	100	0.51242	10.0013	0.00954099	59.1206	0.499515	3.20645	50.0582	0.405983	40593
164.838	25.0132	1651.79	165.025	0.157583	100	0.571977	10.0004	0.00954013	61.9635	0.429401	3.20926	50.0604	0.344634	34462
193.747	30.0116	1299.81	185.476	0.124027	100	0.643771	10.0023	0.00954194	92.833	0.343527	3.24009	50.0903	0.271248	27118.5
222.189	35.0011	950.666	174.441	0.0906726	100	0.71464	9.99798	0.00953781	154.517	0.257905	3.30174	50.1512	0.198301	19834.1
251.519	39.9912	614.597	140.114	0.0586314	100	0.783538	10.0001	0.00953981	233.111	0.175519	3.3803	50.2272	0.128227	12822.6
281.346	44.9809	362.49	89.9761	0.0345817	100	0.835335	10.0003	0.00954007	390.177	0.113844	3.53734	50.3792	0.0756303	7562.77
312.28	49.9928	159.962	42.5137	0.0152634	100	0.877356	10.0022	0.00954184	842.68	0.065737	3.98982	50.8136	0.033381	3337.36

Table C2. DMA results for Remet PC-15 wax (former RR-15).

Time	Temp.	Youngs Storage Modulus	Youngs Loss Modulus	Stress	Freq.	Drive Force	Amplitude	Strain	Displacement	Static Force	Position	Length	Force	Stiffness
(min)	(°C)	(MPa)	(MPa)	(MPa)	(Hz)	(N)	(µm)	(%)	(µm)	(N)	(mm)	(mm)	(N)	(N/m)
22.5783	-0.0253868	2414.88	182.122	0.45279	0.1	0.937148	19.9982	0.01875	10.716	1.4487	3.47696	50.011	0.945324	47270.4
46.2017	5.01196	2202.02	197.449	0.412872	0.1	0.85643	19.9979	0.0187497	15.1184	1.34428	3.48133	50.0159	0.861984	43103.7
68.9107	9.99137	1933.31	204.661	0.362608	0.1	0.754356	20.0045	0.0187559	17.4574	1.19733	3.48364	50.0184	0.757045	37843.7
95.1933	15.0116	1636.76	228.904	0.306989	0.1	0.642238	20.0045	0.0187559	17.8374	1.0129	3.48397	50.0194	0.640925	32039
122.194	20.01	1293.57	212.003	0.242779	0.1	0.51062	20.0176	0.0187681	10.8538	0.80407	3.47693	50.013	0.506868	25321.2
149.575	25.0119	934.94	183.88	0.175412	0.1	0.37176	20.0109	0.0187619	-10.8374	0.582558	3.45519	49.9922	0.366221	18301.1
178.108	30.0123	637.233	137.277	0.119525	0.1	0.254697	20.0056	0.0187569	-29.8802	0.400474	3.4361	49.9731	0.249542	12473.6
206.342	35.0059	375.76	86.3268	0.0703411	0.1	0.150629	19.9659	0.0187197	13.0895	0.237851	3.47903	50.0168	0.146857	7355.36
232.254	39.9968	202.874	47.4921	0.0380556	0.1	0.0817423	20.0071	0.0187583	143.608	0.128759	3.60952	50.1472	0.0794517	3971.18
258.269	44.9976	91.1625	25.1729	0.0170923	0.1	0.0372194	19.9974	0.0187492	433.705	0.058096	3.8996	50.4376	0.0356848	1784.47
287.186	49.9962	23.8368	8.5778	0.00449185	0.1	0.0101482	20.0987	0.0188442	1737.73	0.013391	5.20362	51.8333	0.00937799	466.596
20.2076	-0.0200101	2528.07	166.184	0.473428	0.32	0.978639	19.9736	0.0187269	11.26	1.49586	3.47751	50.0106	0.988413	49485.9
43.6608	4.9913	2328.28	171.877	0.436793	0.32	0.904305	20.0093	0.0187604	17.2343	1.42832	3.48347	50.0175	0.911927	45575.2
66.3696	9.95998	2087.36	187.232	0.391934	0.32	0.813451	20.0265	0.0187765	20.3927	1.29149	3.4866	50.0208	0.818272	40859.4
92.4834	14.9942	1791.25	203.987	0.336141	0.32	0.70039	20.015	0.0187657	21.9785	1.10934	3.48814	50.0228	0.701788	35063.1
119.481	20.0003	1446.67	212.52	0.271621	0.32	0.569349	20.0255	0.0187756	17.0085	0.90022	3.48311	50.0192	0.567084	28318.1
146.525	24.9981	1083.91	191.888	0.203605	0.32	0.429626	20.0349	0.0187844	-1.01179	0.678758	3.46504	50.0027	0.425083	21217.1
175.227	29.9991	745.774	146.502	0.140108	0.32	0.297236	20.0377	0.018787	-20.6884	0.467178	3.44531	49.983	0.292515	14598.2
203.459	34.9993	453.058	101.448	0.0851701	0.32	0.182031	20.0505	0.018799	23.5002	0.289466	3.48945	50.0251	0.177816	8868.44
229.536	40	240.758	58.3993	0.0452107	0.32	0.0972269	20.0286	0.0187785	152.831	0.155676	3.61875	50.1543	0.0943899	4712.75
255.536	44.994	109.924	29.5528	0.0206022	0.32	0.0447235	19.9899	0.0187421	441.975	0.0718859	3.90787	50.4405	0.0430128	2151.73
281.6	49.9926	32.2374	10.8335	0.00604506	0.32	0.0134936	20.0001	0.0187517	1521.93	0.021474	4.98781	51.5211	0.0126207	631.034
13.893	0.0136531	2600.28	166.211	0.487618	1	1.00733	20.001	0.0187525	9.8712	1.54057	3.47614	50.0104	1.01804	50899.4
39.017	4.94825	2453.93	165.634	0.460109	1	0.951402	19.9981	0.0187499	18.4634	1.49239	3.48472	50.0189	0.960605	48034.8
61.7257	9.94548	2215.67	178.051	0.415629	1	0.86124	20.0075	0.0187586	22.0927	1.35563	3.48831	50.0228	0.867741	43370.8
86.1688	14.9501	1948.06	192.694	0.365465	1	0.759538	20.0095	0.0187605	25.2353	1.18963	3.49141	50.0261	0.76301	38132.4
111.496	19.9496	1625.18	202.018	0.304942	1	0.63654	20.0127	0.0187636	24.7028	1.00204	3.49083	50.0261	0.63665	31812.3
138.54	24.9626	1235.72	202.223	0.231658	1	0.487197	19.9948	0.0187468	11.8601	0.764189	3.47793	50.0142	0.483649	24188.7
166.406	29.965	866.366	167.106	0.162394	1	0.343901	19.9922	0.0187443	-6.0261	0.537876	3.45999	49.9968	0.339043	16958.8
196.309	34.9782	534.077	110.692	0.100053	1	0.212841	19.9809	0.0187338	33.9653	0.336128	3.49993	50.037	0.208888	10454.4
223.221	39.9761	288.642	65.3018	0.0541269	1	0.115769	20.0007	0.0187523	164.67	0.18511	3.6306	50.1678	0.113005	5650.05

Time	Temp.	Youngs Storage Modulus	Youngs Loss Modulus	Stress	Freq.	Drive Force	Amplitude	Strain	Displacement	Static Force	Position	Length	Force	Stiffness
(min)	(°C)	(MPa)	(MPa)	(MPa)	(Hz)	(N)	(µm)	(%)	(µm)	(N)	(mm)	(mm)	(N)	(N/m)
250.057	44.9724	133.278	32.5063	0.0250081	1	0.0537752	20.0131	0.0187639	447.422	0.0857401	3.91332	50.451	0.0522114	2608.86
276.119	50.007	40.8343	12.2927	0.00766254	1	0.0167536	20.0142	0.0187649	1541.06	0.0267092	5.00695	51.5467	0.0159977	799.317
13.4013	0.0286729	2707.69	161.312	0.507425	3.2	1.04572	19.9878	0.0187402	11.0436	1.6017	3.47732	50.0111	1.05939	53002
38.64	4.94988	2558.97	159.619	0.480042	3.2	0.990078	20.0081	0.0187592	19.871	1.55257	3.48614	50.0202	1.00222	50090.8
61.3302	9.94655	2337.73	164.157	0.438579	3.2	0.905862	20.0099	0.0187609	24.0338	1.42693	3.49027	50.0245	0.915655	45760.1
85.7533	14.957	2072.65	176.474	0.388847	3.2	0.804929	20.0098	0.0187608	27.6611	1.26165	3.49386	50.0284	0.811826	40571.4
111.062	19.9489	1766.87	192.674	0.331524	3.2	0.688648	20.0126	0.0187634	28.7559	1.0917	3.49491	50.0299	0.692149	34585.8
138.07	24.9566	1393.46	199.598	0.261448	3.2	0.54607	20.0116	0.0187625	18.7618	0.867506	3.48486	50.0208	0.545844	27276.4
165.937	29.97	998.902	176.349	0.187425	3.2	0.393837	20.0122	0.0187631	2.43386	0.623414	3.46847	50.0053	0.391302	19553.1
195.858	34.9837	625.782	125.221	0.117404	3.2	0.247649	20.0102	0.0187612	42.8516	0.392533	3.50883	50.0454	0.245114	12249.4
222.807	39.9659	343.431	79.9512	0.0644329	3.2	0.13635	20.0105	0.0187615	174.166	0.218686	3.6401	50.177	0.134522	6722.53
249.642	44.9831	158.549	40.0204	0.0297472	3.2	0.0624805	20.0112	0.0187622	457.593	0.102557	3.9235	50.4601	0.0621056	3103.53
275.701	50.0044	51.1409	15.2087	0.00959376	3.2	0.0193966	20.0083	0.0187594	1559.02	0.0334248	5.02491	51.5686	0.0200296	1001.06
11.7295	0.0449494	2798.81	161.64	0.524856	10	1.0644	20.0012	0.0187528	11.4401	1.66067	3.47773	50.0119	1.09578	54785.7
37.663	4.94268	2670.81	160.319	0.500968	10	1.0159	20.0059	0.0187572	21.1376	1.61026	3.48742	50.0215	1.04591	52280
60.353	9.94521	2449.32	161.932	0.459434	10	0.931544	20.0064	0.0187576	25.5721	1.48582	3.49182	50.026	0.959196	47944.4
84.4375	14.9597	2193.51	169.002	0.411437	10	0.834059	20.0058	0.018757	30.0382	1.3318	3.49625	50.0308	0.85899	42937.1
109.746	19.9456	1905.47	181.085	0.357406	10	0.724352	20.0056	0.0187569	32.5538	1.17096	3.49873	50.0336	0.746184	37298.8
136.588	24.9453	1545.71	196.537	0.28995	10	0.587489	20.0072	0.0187584	25.254	0.956326	3.49137	50.027	0.605351	30256.7
164.285	29.9616	1136.29	184.681	0.213077	10	0.430207	20.0003	0.0187519	11.9958	0.706302	3.47805	50.0146	0.444857	22242.5
194.207	34.9641	723.636	139.656	0.135712	10	0.269713	20.0028	0.0187542	52.7273	0.450196	3.51872	50.0562	0.283337	14164.9
221.324	39.9549	406.922	89.6344	0.0763322	10	0.14521	20.0072	0.0187584	186.119	0.258377	3.65206	50.1898	0.159365	7965.35
248.326	44.9746	191.036	47.3113	0.0358588	10	0.059717	20.0204	0.0187707	470.152	0.123319	3.93606	50.4749	0.0748652	3739.45
274.385	50.0007	63.7457	17.1156	0.0120347	10	0.0104189	20.1361	0.0188792	1598.74	0.0415923	5.06463	51.6072	0.0251258	1247.8
11.3838	0.0593423	2908.96	166.977	0.545325	31.6	0.93841	19.9944	0.0187464	12.5223	1.72527	3.47883	50.0126	1.13852	56941.7
37.411	4.94213	2783.82	166.177	0.522183	31.6	0.891426	20.0065	0.0187578	22.1208	1.66142	3.48842	50.0222	1.0902	54492.2
60.101	9.94624	2561.87	166.731	0.480591	31.6	0.807108	20.0083	0.0187594	26.8118	1.53943	3.49308	50.0269	1.00337	50147.6
84.147	14.9458	2309.58	168.936	0.433279	31.6	0.711129	20.009	0.0187601	32.1032	1.40465	3.49833	50.0323	0.904591	45209.1
109.455	19.9476	2036.55	176.046	0.38204	31.6	0.607328	20.0081	0.0187592	35.3918	1.25025	3.50158	50.0356	0.797616	39864.7
136.279	24.9491	1691.42	193.758	0.317293	31.6	0.476909	20.0078	0.018759	29.6373	1.04501	3.49578	50.0295	0.662438	33108.9
163.957	29.9592	1279.91	193.361	0.240133	31.6	0.321418	20.0108	0.0187617	18.8734	0.794966	3.48495	50.0189	0.501345	25053.7
193.861	34.9674	836.346	159.446	0.156922	31.6	0.154496	20.0119	0.0187628	61.842	0.52011	3.52785	50.0617	0.327618	16371.2
221.016	39.9544	477.81	101.682	0.0896069	31.6	0.0439531	20.0022	0.0187537	195.711	0.302058	3.66167	50.1957	0.187079	9352.95

Time	Temp.	Youngs Storage Modulus	Youngs Loss Modulus	Stress	Freq.	Drive Force	Amplitude	Strain	Displacement	Static Force	Position	Length	Force	Stiffness
(min)	(°C)	(MPa)	(MPa)	(MPa)	(Hz)	(N)	(µm)	(%)	(µm)	(N)	(mm)	(mm)	(N)	(N/m)
248.035	44.978	230.478	57.1574	0.0432072	31.6	0.100122	19.9949	0.0187468	481.186	0.14856	3.9471	50.4828	0.0902071	4511.51
274.09	50.0011	78.7469	21.0348	0.014771	31.6	0.156435	20.0063	0.0187576	1626.07	0.0519498	5.09197	51.6728	0.0308386	1541.44
10.417	0.0605872	3051.68	171.297	0.572471	100	0.650083	20.0081	0.0187592	11.7995	1.79009	3.47813	50.0114	1.19519	59735.5
36.8925	4.93866	2935.32	172.403	0.550546	100	0.694011	20.0046	0.018756	21.4609	1.6757	3.48776	50.0193	1.14942	57457.7
59.5825	9.93684	2714.73	177.898	0.509157	100	0.777819	20.004	0.0187554	26.1753	1.5589	3.49244	50.0242	1.06301	53139.8
83.4563	14.9437	2465.66	180.806	0.462368	100	0.872485	20.0007	0.0187523	31.5821	1.46463	3.49783	50.031	0.965322	48264.4
108.765	19.9512	2199.67	184.173	0.412487	100	0.974021	20.0006	0.0187522	34.2408	1.31423	3.50045	50.0335	0.861181	43057.8
135.588	24.945	1867.12	202.026	0.350126	100	1.1018	20.0007	0.0187522	25.701	1.09902	3.49186	50.014	0.730986	36548.1
163.096	29.9459	1460.14	210.321	0.27377	100	1.25821	19.9978	0.0187496	14.4168	0.875544	3.48052	49.9982	0.57157	28581.6
192.83	34.9594	992.924	189.15	0.186192	100	1.43824	20.0002	0.0187519	56.3861	0.616689	3.52242	50.031	0.388727	19436.1
220.07	39.9587	585.474	123.845	0.10977	100	1.59499	19.9971	0.0187489	190.192	0.390724	3.65617	50.1554	0.229175	11460.4
247.174	44.9894	300.191	73.6784	0.056293	100	1.70591	20.0008	0.0187524	473.123	0.230543	3.93906	50.4019	0.117527	5876.13
273.316	50	116.897	37.5286	0.0219203	100	1.77724	20.0001	0.0187517	1707.72	0.134269	5.17363	51.4832	0.0457646	2288.22

Table C3. DMA results for Cerita F20-844B wax (former green XP wax).

Time	Temp.	Youngs Storage Modulus	Youngs Loss Modulus	Stress	Freq.	Drive Force	Amplitude	Strain	Displacement	Static Force	Position	Length	Force	Stiffness
(min)	(°C)	(MPa)	(MPa)	(MPa)	(Hz)	(N)	(µm)	(%)	(µm)	(N)	(mm)	(mm)	(N)	(N/m)
42.6148	8.94E-05	1988.89	178.813	0.281969	0.01	0.595072	14.968	0.0141772	63.1875	0.732842	3.32199	50.0627	0.602704	40266.2
113.011	4.99074	1807.62	215.319	0.256713	0.01	0.544332	14.9938	0.0142017	69.4312	0.690996	3.32822	50.0692	0.548718	36596.2
182.816	9.99434	1532.44	244.559	0.217796	0.01	0.465482	15.0052	0.0142124	72.7641	0.589271	3.33151	50.0725	0.465536	31025
258.73	14.9929	1180.05	251.074	0.167453	0.01	0.362448	14.9819	0.0141904	74.0709	0.453449	3.33275	50.0738	0.357929	23890.7
338.671	19.9966	792.688	205.852	0.112492	0.01	0.246913	14.9828	0.0141912	69.7036	0.31072	3.32833	50.0698	0.24045	16048.4
418.239	25.0048	494.958	115.129	0.0702972	0.01	0.15378	14.9949	0.0142026	59.0341	0.195113	3.31761	50.0594	0.150259	10020.7
499.799	30.0005	313.251	77.3613	0.044501	0.01	0.0978793	14.9986	0.0142062	67.9859	0.123824	3.32653	50.0673	0.09512	6341.93
579.116	35.001	161.479	43.0085	0.0229613	0.01	0.0508859	15.0125	0.0142194	124.089	0.0644239	3.38261	50.1223	0.0490794	3269.22
674.293	39.9997	59.4351	22.4397	0.00845355	0.01	0.0194643	15.0165	0.0142232	380.101	0.0242904	3.6386	50.3702	0.0180693	1203.29
863.594	45	18.7956	11.9458	0.00267673	0.01	0.0068944	15.0356	0.0142413	4493.44	0.0079999	7.75193	54.497	0.00572145	380.526
994.389	50	37.7975	21.1172	0.00536504	0.01	0.0132529	14.9859	0.0141942	10759.2	0.0158361	14.0177	60.6508	0.0114677	765.231
55.9863	-1.10E-03	2110.83	143.178	0.299456	0.03	0.630232	14.978	0.0141867	65.3916	0.758211	3.32421	50.0646	0.640082	42734.8
128.053	5.00476	1949.46	174.539	0.276737	0.03	0.584221	14.9874	0.0141956	71.5429	0.707855	3.33034	50.0708	0.591521	39467.8
197.857	10.0031	1693.91	213.657	0.240435	0.03	0.510697	14.9858	0.0141941	75.5284	0.610572	3.33428	50.0744	0.513925	34294.1
280.499	14.9996	1360.53	239.43	0.193099	0.03	0.414391	14.9847	0.014193	81.836	0.513583	3.34055	50.05	0.412746	27544.5
360.439	20.0012	947.025	221.085	0.134382	0.03	0.292736	14.9814	0.0141899	76.9412	0.347267	3.33558	50.0235	0.287238	19173
438.336	24.9997	575.966	136.211	0.0818016	0.03	0.178951	14.9947	0.0142025	61.8098	0.218564	3.32039	49.9992	0.174849	11660.7
519.897	30.0021	366.347	83.6482	0.0520457	0.03	0.113918	14.9991	0.0142067	76.299	0.133801	3.33485	50.0275	0.111247	7416.88
597.533	35.0014	189.827	47.3868	0.0269935	0.03	0.0595391	15.0132	0.01422	134.088	0.0671501	3.39261	50.1271	0.0576982	3843.15
691.034	39.998	73.4129	23.2565	0.0104327	0.03	0.0235398	15.0036	0.0142109	415.279	0.0267853	3.67378	50.4025	0.0222996	1486.28
903.698	45.0001	32.4972	16.6376	0.00457822	0.03	0.0111126	14.8739	0.014088	4532.05	0.0114323	7.79055	54.5047	0.00978586	657.923
1011.11	50	51.3867	27.5942	0.00731458	0.03	0.0178578	15.0284	0.0142344	10792.2	0.0184876	14.0507	60.7792	0.0156348	1040.35
59.607	0.00118333	2198	116.502	0.312315	0.1	0.656212	15.0016	0.014209	66.6012	0.789952	3.32543	50.0662	0.667569	44499.7
131.842	5.00332	2064.38	133.978	0.293131	0.1	0.617045	14.9915	0.0141994	73.0277	0.741836	3.33183	50.0726	0.626561	41794.5
201.648	10.0049	1846.9	181.4	0.262227	0.1	0.554528	14.9902	0.0141982	77.6034	0.654324	3.33637	50.0769	0.560505	37391.4
285.028	14.9958	1547.57	214.036	0.219852	0.1	0.468315	14.9987	0.0142063	88.5661	0.606682	3.34732	50.0726	0.469929	31331.3
365.132	19.9966	1128.36	229.94	0.160223	0.1	0.346309	14.9917	0.0141997	87.3963	0.451856	3.34608	50.0429	0.342475	22844.2
442.855	24.9934	683.32	161.773	0.0970449	0.1	0.212083	14.9942	0.014202	66.7656	0.251344	3.32536	50.0085	0.207432	13834.2
524.417	29.9966	428.218	93.5064	0.060846	0.1	0.1328	15.0017	0.0142091	83.8136	0.170703	3.34238	50.0406	0.130057	8669.5
602.052	34.9935	226.105	54.6241	0.03214	0.1	0.0707055	15.0075	0.0142146	148.969	0.0904469	3.4075	50.1406	0.0686986	4577.62
695.195	40.0034	90.1281	24.333	0.012796	0.1	0.0284737	14.9896	0.0141976	430.796	0.0321553	3.6893	50.427	0.0273513	1824.69
907.842	44.9999	43.9507	22.6449	0.00629075	0.1	0.0152464	15.1116	0.0143132	4558.85	0.0164027	7.81735	54.5517	0.0134464	889.806

Time	Temp.	Youngs Storage Modulus	Youngs Loss Modulus	Stress	Freq.	Drive Force	Amplitude	Strain	Displacement	Static Force	Position	Length	Force	Stiffness
(min)	(°C)	(MPa)	(MPa)	(MPa)	(Hz)	(N)	(µm)	(%)	(µm)	(N)	(mm)	(mm)	(N)	(N/m)
1015.08	50.0003	71.0226	39.4213	0.0100878	0.1	0.024767	14.9959	0.0142036	10816.9	0.0257837	14.0754	60.8103	0.0215625	1437.89
65.3113	3.68E-04	2280.26	97.1004	0.323783	0.32	0.679476	14.9914	0.0141994	68.2957	0.82	3.32714	50.0677	0.69208	46165.1
137.546	4.99895	2155.31	111.923	0.306103	0.32	0.643348	14.9945	0.0142023	74.9843	0.773022	3.3338	50.0743	0.65429	43635.4
208.189	10.0006	1960.38	140.323	0.27834	0.32	0.586691	14.9902	0.0141983	81.2723	0.697319	3.34006	50.08	0.594946	39688.9
291.569	14.9948	1697.35	182.031	0.241017	0.32	0.510797	14.9917	0.0141996	92.0532	0.618316	3.35081	50.0907	0.51517	34363.8
375.066	19.9983	1294.36	218.855	0.183738	0.32	0.394068	14.9871	0.0141953	96.2912	0.485624	3.35499	50.0722	0.392737	26205
452.788	24.9979	833.657	193.261	0.118383	0.32	0.258056	14.9925	0.0142004	78.0133	0.315591	3.33664	50.0166	0.253041	16877.8
534.35	29.9964	497.053	108.261	0.0705826	0.32	0.153907	14.9923	0.0142002	101.645	0.188517	3.36022	50.0546	0.150869	10063.1
611.149	35.0005	269.892	63.6364	0.0383412	0.32	0.0841663	14.9986	0.0142061	169.538	0.103027	3.42807	50.1574	0.0819537	5464.11
703.438	39.9971	105.647	26.7698	0.0150069	0.32	0.0332192	14.9972	0.0142049	466.724	0.0379533	3.72523	50.4529	0.0320771	2138.87
916.9	45	59.5246	27.9845	0.00849456	0.32	0.0201788	15.0667	0.0142707	4654.93	0.0217919	7.91343	54.6207	0.018157	1205.11
1022.46	50.0007	96.6304	54.4796	0.0137611	0.32	0.0338604	15.0353	0.0142409	10902.5	0.0353396	14.161	60.8714	0.029414	1956.33
66.7068	0.00642797	2338.49	88.374	0.332152	1	0.696432	14.996	0.0142037	69.1259	0.846469	3.32798	50.0689	0.709969	47344
138.942	4.99423	2221.84	92.9162	0.315632	1	0.662558	14.9983	0.0142059	76.0217	0.801586	3.33485	50.0758	0.674658	44982.3
209.605	9.99731	2054.31	114.674	0.291817	1	0.613863	14.9974	0.0142051	82.7656	0.735946	3.34157	50.0823	0.623754	41590.7
292.985	14.9984	1821	149.678	0.258668	1	0.54621	14.9971	0.0142048	93.7008	0.651669	3.35247	50.0932	0.552899	36867
376.607	20.0044	1435.54	197.79	0.203884	1	0.434572	14.9948	0.0142026	100.032	0.542637	3.35875	50.0804	0.435798	29063.3
454.31	24.9949	983.535	209.012	0.139712	1	0.302782	14.9975	0.0142051	83.9427	0.368015	3.34259	50.04	0.298632	19912.2
535.872	30.0121	575.363	130.365	0.0817414	1	0.178319	14.9994	0.0142069	104.084	0.217725	3.36267	50.0654	0.174721	11648.5
612.67	35.0003	318.086	72.6279	0.0451909	1	0.0988643	14.9996	0.0142071	177.51	0.122124	3.43605	50.1715	0.0965948	6439.81
704.924	39.9977	123.945	31.2501	0.0175974	1	0.0388047	14.9897	0.0141977	476.449	0.0444863	3.73496	50.4742	0.0376142	2509.34
918.323	45.0002	77.3532	35.2581	0.0109393	1	0.0257216	14.9308	0.014142	4675.21	0.0270406	7.93371	54.6713	0.0233825	1566.06
1023.98	49.9998	134.713	74.0735	0.0191585	1	0.046727	15.015	0.0142217	10936.5	0.0499419	14.195	60.9288	0.0409509	2727.33
67.8525	-7.08E-04	2401.56	85.1793	0.341106	3.2	0.713476	14.9958	0.0142035	70.0425	0.870605	3.3289	50.0697	0.729109	48620.9
140.088	4.99653	2287.02	85.2748	0.324855	3.2	0.680132	14.9966	0.0142043	77.1401	0.827311	3.33598	50.0768	0.694372	46301.9
210.921	10	2125.15	100.274	0.301862	3.2	0.633042	14.9966	0.0142043	84.7911	0.767804	3.34361	50.0841	0.645224	43024.7
294.301	15.0035	1918.8	128.596	0.272513	3.2	0.573037	14.9945	0.0142023	96.6353	0.687743	3.35542	50.0957	0.582492	38847.1
377.925	19.9977	1584.45	171.706	0.224937	3.2	0.475866	14.9884	0.0141966	103.956	0.565458	3.36269	50.1023	0.4808	32078
456.352	25.004	1143.91	210.344	0.162435	3.2	0.348388	14.9921	0.0142	101.139	0.429897	3.35981	50.0601	0.347201	23159
537.913	30.0008	681.5	157.666	0.0967794	3.2	0.209933	14.9931	0.0142009	123.388	0.256568	3.38199	50.0355	0.206864	13797.3
614.711	35.0071	371.604	82.4956	0.0527844	3.2	0.114046	14.9968	0.0142045	191.923	0.141016	3.45047	50.1815	0.112826	7523.32
706.79	40.0006	146.835	39.5212	0.0208522	3.2	0.0449714	14.9933	0.0142011	502.716	0.0564361	3.76123	50.4908	0.0445713	2972.75
919.818	45.0001	101.698	45.3787	0.0141319	3.2	0.032037	14.6711	0.0138959	4742.59	0.0345629	8.00109	54.7162	0.0302066	2058.92

Time	Temp.	Youngs Storage Modulus	Youngs Loss Modulus	Stress	Freq.	Drive Force	Amplitude	Strain	Displacement	Static Force	Position	Length	Force	Stiffness
(min)	(°C)	(MPa)	(MPa)	(MPa)	(Hz)	(N)	(µm)	(%)	(µm)	(N)	(mm)	(mm)	(N)	(N/m)
1025.47	49.9985	177.085	96.1464	0.0252358	3.2	0.0603118	15.0456	0.0142507	11040.8	0.0662395	14.2994	61.0042	0.053941	3585.17
68.248	0.0175263	2455.32	82.3486	0.348797	10	0.716654	14.9982	0.0142058	70.6713	0.892613	3.32954	50.0705	0.745547	49709.3
140.483	4.97928	2343.86	82.2863	0.332947	10	0.684161	14.9975	0.0142051	77.8492	0.850584	3.3367	50.0776	0.711668	47452.6
211.336	10.0073	2188.88	88.0828	0.310932	10	0.639003	14.9975	0.0142051	85.8268	0.794748	3.34466	50.0855	0.664612	44315
294.716	14.997	2000.27	107.406	0.284136	10	0.584103	14.9973	0.0142049	98.2558	0.720688	3.35705	50.0978	0.607335	40496.4
378.341	20.0086	1699.37	147.768	0.241378	10	0.496691	14.9963	0.014204	106.618	0.604379	3.36537	50.1058	0.51594	34404.6
456.791	24.9837	1295.75	198.777	0.184025	10	0.380029	14.9944	0.0142022	104.51	0.460485	3.3632	50.1031	0.39335	26233.1
538.454	29.9932	804.88	179.462	0.114353	10	0.23544	15	0.0142075	131.527	0.296744	3.39014	50.0492	0.244428	16295.2
615.252	34.9949	433.423	95.5505	0.0615622	10	0.121012	14.996	0.0142037	200.697	0.163945	3.45926	50.1939	0.131588	8774.87
707.277	40.005	176.95	49.7598	0.0251638	10	0.0429877	15.0141	0.0142208	509.442	0.0625439	3.76796	50.5057	0.0537873	3582.46
920.241	44.9999	128.27	57.128	0.0183804	10	0.0313126	15.1288	0.0143295	4784.06	0.0456071	8.04257	54.7744	0.0392878	2596.89
1025.92	49.999	239.79	128.739	0.0341676	10	0.0713378	15.0438	0.014249	11099.7	0.0888109	14.3582	61.0847	0.0730327	4854.68

Appendix D. Energy Savings

The cost savings due to the introduction of this technology will primarily come from the increased yield and the elimination of trial and error in the casting design process. This will lead to reduced material and energy needs, and economic benefits. The tools developed will also considerably improve overall productivity and expand markets, although these are somewhat difficult to quantify. Only the energy benefits will be used in calculating energy and environmental savings.

The increased demands for the consolidation of components into fewer parts and the emphasis on net-shape parts makes investment casting increasingly attractive for the production of high precision-high integrity castings. In addition, need to increase consistency in investment castings and reduce costs by improving yields and eliminating rework justifies the development of tools for predicting pattern tooling and casting dimensions in investment casting. A large part of the investment casting industry deals with high value iron, nickel, and cobalt-base alloys.

In this program, plant procedures and computational methodologies will be provided to dramatically improve dimensional accuracy of castings through the use of computer simulations. Improving dimensioning practices will reduce the downtime due to mold rework, allow the use of thinner walls by controlling their deformation, increase productivity of the design process, less parts will need machining. Aside from improved casting dimensions, the process analysis will provide information investment casting process that will allow lowering the pouring temperatures assess the effect of wax or shell systems. The technology will specifically result in the following benefits:

- Energy efficiency through scrap reduction and yield increase; (More parts with have their dimensions within blueprint tolerances)
- Pour Molten metal at lower temperatures, resulting from through process analysis.
- Reduced downtime due to mold reworks; Furnace idling; Lost furnace heat. Die rework, and ensuing downtime will be eliminated.
- Less metal: Thinner walls, More structural geometry, less mass, resulting from through process analysis
- Productivity improvements; Less cutting, grinding, rework, heat treat, (More parts with have their dimensions within blueprint tolerances and less part features will need machining)

Assumptions: Scrap deduction from 4% to 3%. And increase in yield from 55 to 65%.
Baseline Metric: Existing alloy Melting BTU's/Ton Produced for Investment Casting (IC):

HA Steel; IC	32.8×10^6 BTU/Ton Produced x 120,775 Tons Produced/yr	=	3.96×10^{12} BTU/yr
Titanium; IC	35.0×10^6 BTU/Ton Produced x 8,627 Tons Produced/yr	=	0.30×10^{12} BTU/yr
Aluminum; IC	7.5×10^6 BTU/Ton Produced x 43,134 Tons Produced/yr	=	0.32×10^{12} BTU/yr
			4.58×10^{12} BTU/yr

New technology would enable reductions in scrap for all alloy families from 4% to 3%, on average
New technology would enable in increase in yield for all alloy families from 55% to 65% on average

New/Old Ratio will be the same for all alloys so it will be determined first:

All IC alloys 165,900 Tons Shipped x 1.03 (Tons Shipped + Scrap)/Tons Shipped = 170,877 Tons Produced
170,877 Tons Produced / ((55% existing yield + 10% yield increase)/100) = 262,888 Tons Melted
262,888 Tons Melted New Technology / 313,702 Tons Melted Old Technology = 0.838 New/Old Ratio

- HA steel 116,130 Tons Shipped x 1.03 (Tons Shipped + Scrap)/Tons Shipped = 119,614 New Tons Produced
  119,614 Tons Produced / ((55% existing yield + 10% yield increase)/100) = 184,021 New Tons Melted
  0.838 New/Old Ratio x (32.8×10^6 Old Melting BTU/Ton Produced) = $27{,}5 \times 10^6$ New Melting BTU/Ton Produced
  27.5×10^6 New Melting BTU/Ton Produced x 119,614 New Tons Produced/yr = 3.29×10^{12} BTU/yr
- Ti 8,295 Tons Shipped x 1.03 (Tons Shipped + Scrap)/Tons Shipped = 8,544 New Tons Produced
  8,544 Tons Produced / ((55% existing yield + 10% yield increase)/100) = 13,145 New Tons Melted
  0.838 New/Old Ratio x (35.0×10^6 Old Melting BTU/Ton Produced) = 29.33×10^6 New Melting BTU/Ton Produced
  29.33×10^6 New Melting BTU/Ton Produced x 8,544 New Tons Produced/yr = 0.25×10^{12} BTU/yr
- Al 43,134 Tons Shipped x 1.03 (Tons Shipped + Scrap)/Tons Shipped = 43,719 New Tons Produced
  43,719 Tons Produced / ((55% existing yield + 10% yield increase)/100) = 65,722 New Tons Melted
  0.838 New/Old Ratio x (7.5×10^6 Old Melting BTU/Ton Produced) = 6.29×10^6 New Melting BTU/Ton Produced
  6.29×10^6 New Melting BTU/Ton Produced x 43,719 New Tons Produced/yr = 0.28×10^{12} BTU/yr

Table D.1. Comparison of energy used and energy saved for existing versus new technology

Investment casting material	Assumptions	Energy used/saved ($\times 10^{12}$ Btu/year)
Baseline metric		
HA steel	32.8×10^6 Btu/ton x 120,775 tons/year	3.96
Titanium	35.0×10^6 Btu/ton x 8,627 tons/year	0.30
Aluminum	7.5×10^6 Btu/ton x 43,134 tons/year	0.32
Total energy use, baseline		4.58
New technology metric		
HA steel	27.5×10^6 Btu/ton x 119,614 tons/year	3.29
Titanium	29.3×10^6 Btu/ton x 8,544 tons/year	0.25
Aluminum	6.29×10^6 Btu/ton x 43,719 tons/year	0.28
Total energy use, new technology		3.82
Energy savings		**0.76**